Journal of Earth Science, Vol. 36, No. 4, p. 1568–1590, August 2025 *ISSN 1674-487X*
Printed in China
https://doi.org/10.1007/s12583-022-1673-6

Origin of Burrow-Associated Dolomites and Its Reservoir Implications: A Case Study from the Lower–Middle Ordovician Carbonates of Tarim Basin (NW China)

Chuan Guo[1, 2, 3], **Daizhao Chen**[3, 4], **Yong Fu**[1, 2], **Xiqiang Zhou**[3, 4], **Cunge Liu**[*5]

1. *College of Resources and Environmental Engineering*, *Key Laboratory of Karst Georesources and Environment*, *Ministry of Education*, *Guizhou University*, *Guiyang* 550025, *China*
2. *Guizhou Karst Environmental Ecosystems Observation and Research Station*, *Ministry of Education*, *Guizhou* 550025, *China*
3. *Institutions of Earth Science*, *Chinese Academy of Sciences*, *Beijing* 100029, *China*
4. *University of Chinese Academy of Sciences*, *Beijing* 100049, *China*
5. *Guangdong University of Petrochemical Technology*, *Maoming* 525000, *China*

ABSTRACT: The Yingshan Formation of the Lower–Middle Ordovician in the Tarim Basin (NW China) was mainly deposited in a shallow platform, which was intensely bioturbated with burrows filled with both dolomites and calcites. This study aims to figure out the controls on the dolomitization of burrow infills and the effects on petroleum reservoir quality based on petrographic examination, fluid inclusion microthermometry, and isotopic (C-O-Sr) geochemical analyses. The differentiation of burrow-associated carbonates (dolomites and calcites) was likely controlled by the interactions of sea-level oscillations of variable orders and depositional environments. The burrow-associated dolomites (BADs) were precipitated in a relatively restricted (i.e., lagoon) depositional environment during the lowstand of long-term sea level. In contrast, the burrow-associated calcites (BACs) were formed in a water circulation-improved lagoonal environment during the transgression of long-term sea level. Isotopic geochemical data indicate that the BADs in the Yingshan Formation were formed from slightly saline (i.e., mesosaline to penesaline) seawater, whereas the BACs were precipitated from nearly normal seawater. In addition to the anoxic condition, the presence of marine-sourced organic matter and sulfate-reducing bacteria, and a sufficient supply of dolomitizing fluids enriched in magnesium ions (Mg^{2+}) and their Mg^{2+} concentration may have played a critical role in the formation of BADs. In the more permeable and disturbed burrow sediments as a result of burrowing, penetrating fluids with higher salinities and higher Mg^{2+} concentration relative to seawater favored dolomite precipitation. The fluids with seawater-like Mg^{2+} concentration, however, would lead to calcite precipitation. The progressive dolomitization of these burrowed sediments could have propagated the dolomitizing fronts and extended into ambient limestones, leading to the development of extensive dolomites. This dolomitization process can improve the petrophysical properties (porosity and permeability) and the potential as hydrocarbon reservoirs during the emplacement of hydrocarbons from underlying source rocks of the Cambrian to Lower Ordovician.

KEY WORDS: burrow-associated dolomites, isotopic geochemistry, reservoirs, Tarim Basin, Lower–Middle Ordovician.

0 INTRODUCTION

The dolomite rock is a ubiquitous rock type making up the sedimentary covers of Earth's surface crust and accounts for approximately 50% of the world carbonate reservoirs (Zenger et al., 1980). However, compared with limestones, the origins of ancient massive dolomite rocks have been a matter of extensive disputes since being discovered, although various dolomitization models (including seepage/reflux, freshwater/seawater mixing, microbe-mediated and burial dolomitization) have been proposed to elucidate the formation of extensive dolomites in the geologic record (e.g., Davies and Smith, 2006; Machel, 2004; Warren, 2000; Vasconcelos et al., 1995; Land,

*Corresponding author: Liucunge@163.com

Manuscript received October 9, 2021.
Manuscript accepted April 18, 2022.

Guo Chuan, Chen Daizhao, Fu Yong, Zhou Xiqiang, Liu Cunge, 2025. Origin of Burrow-Associated Dolomites and Its Reservoir Implications: A Case Study from the Lower–Middle Ordovician Carbonates of Tarim Basin (NW China). *Journal of Earth Science*, 36(4): 1568–1590. https://doi.org/10.1007/s12583-022-1673-6. http://en.earth-science.net

1985; Kohout et al., 1977; Adams and Rhodes, 1960). Of these, the origin of mottled burrow-associated dolomites (BADs) has still not been completely understood, although several studies have demonstrated the origin of similar fabrics around the world (e.g., Baniak et al., 2014, 2013; Corlett and Jones, 2012; Rameil, 2008; Gingras et al., 2004a; Horbury and Qing, 2004; Török, 2000). Recently, more attention has been paid to this type of dolomites since dolomitized burrow systems in limestones can serve either as primary or secondary pathways for fluid flows, accelerating later massive dolomitization process of ambient limestones (e. g., Baniak et al., 2014, 2013; Corlett and Jones, 2012; Rameil, 2008; Gingras et al., 2004a). This process can improve the rock petrophysical properties and potentials as hydrocarbon reservoirs (e.g., Baniak et al., 2014, 2013; Gingras et al., 2004a).

The irregular burrow systems are extensively present within the Yingshan Formation of the Early–Middle Ordovician in the Tarim Basin, NW China. These burrow systems are filled with either dolomites or calcites, which resembles the case reported from the Middle Devonian Lonely Bay Formation (Northwest Territories, Canada) by Corlett and Jones (2012). The authors ascribed the distinctive burrow infills at the same stratigraphic intervals to the geochemical differences of diagenetic fluids within individual burrows. In contrast, different types of burrow infills (dolomites vs calcites) generally occur in different stratigraphic levels in the Yingshan Formation, which was seemingly dictated by allogenic forces (i.e., eustatic fluctuations of variable orders and depositional environments). In addition, the Lower Ordovician dolomite rocks occur as the main reservoirs, which have been paid much attention (Hu et al., 2019, 2011; Lan et al., 2018; Zhang et al., 2014; Zheng et al., 2014; Qiao et al., 2012), which improve the understanding of development of the Lower Ordovician dolomites in the Tarim Basin. The origin of the BADs that have heterogeneous porosity within the Yingshan Formation, however, has not been systematically documented hitherto. This case thus offers a precious opportunity to understand the controls on the selective dolomitization or calcitization of burrow infills, the distributional patterns of BADs, and their reservoir implications.

In this paper, detailed macroscopic (field and core observation) and microscopic (conventional optical and cathodoluminescent) petrographic examinations, and isotope geochemistry (C, O, and Sr), and fluid inclusion microthermometry were carried out on the burrow infills in the Lower–Middle Ordovician Yingshan Formation in the Tarim Basin. This study aims to (1) differentiate the BADs and BACs and their tempo-spatial distributional patterns, (2) establish their diagenetic paragenesis, (3) define geochemical attributes of burrow infills and their parental fluids, (4) sort out the mechanisms of selective dolomitization and calcitization of burrow systems, and driving factors, and (5) document the hydrocarbon reservoir potentials of the BADs.

1 GEOLOGICAL SETTING

The Tarim basin is located geographically in northwestern China and bordered by Tianshan Mountain to the north, Kunlun Mountain to the south, and Altun Mountain to the southeast, respectively (Figure 1) (Gao et al., 2021; Zhu et al., 2015). The Tarim Basin has undergone multiple tectonic episodes, including Caledonian, Hercynian, Indosinian, and Himalayan orogenies, leading to intense exhumation, erosion, and subsidence (Jia and Wei, 2002; He et al., 2000; Tang, 1997). Due to the tectonic deformation (or modification), the present-day basin configuration is divided into several structural units, including the North Uplift, North Depression, Central Uplift, and Southeast Depression from north to south (Figure 2), and characterized by the widespread negative relief of the basin surrounded by numerous mountains (or uplifts).

During the Early Ordovician, the basin was located at 30ºS, with a warm, semi-arid to arid climate condition (Scotese and McKerrow, 1990), and then migrated to 20ºS by the Middle Ordovician (Fang and Shen, 2001; Li et al., 1995). During the Early Ordovician, the Tarim Basin was subject to a long-lasting grand transgression and occupied by an extensive shallow-water carbonate platform (Guo et al., 2018b; Feng et al., 2007; Gao et al., 2006). Toward the Middle Ordovician, the united grand carbonate platform was progressively evolved into three smaller carbonate platforms due to the combined effects of sea-level changes, tectonic subsidence, and sediment accumulation (Figure 1) (Guo et al., 2018b; Ren et al., 2015; Yan et al., 2010; Gu et al., 1994). They were separated by two deeper-water interplatformal depressions. In such a depositional context, individual platform interiors were likely represented by relatively restricted depositional environments (i.e., lagoon) with variably-limited water circulation to the open sea. The carbonate depositional system persisted into the early Late Ordovician during which the transgression reached a maximum. Afterward, it was gradually switched to a siliciclastic-dominated system as a result of the succeeding regression (Feng et al., 2007).

The Ordovician stratigraphic units of the shallow-water regime in the Tarim Basin consist of the Penglaiba, Yingshan, Yijianfang, Qiaerbake, Lianglitage, and Sangtamu formations in ascending order (Figure 3). The Penglaiba Formation, about 250 to 600 m thick, is mainly composed of two parts: the lower part of light gray dolomites intercalated with peloidal limestones, and the upper part of light gray peloidal limestones interbedded with dolomites, representing the transition of depositional environments from restricted to less restricted platform (Guo C et al., 2018a; Zhang and Munnecke, 2016; Guo F et al., 2010). The Yingshan Formation, approximately 200 to 1 000 m thick, conformably or unconformably overlies the Penglaiba Formation in different parts of the Tarim Basin. This formation comprises the lower part of gray dolomites intercalated with bioclastic-peloidal limestones of semi-restricted subtidal environments, in which burrow infills were completely dolomitized. In contrast, the upper

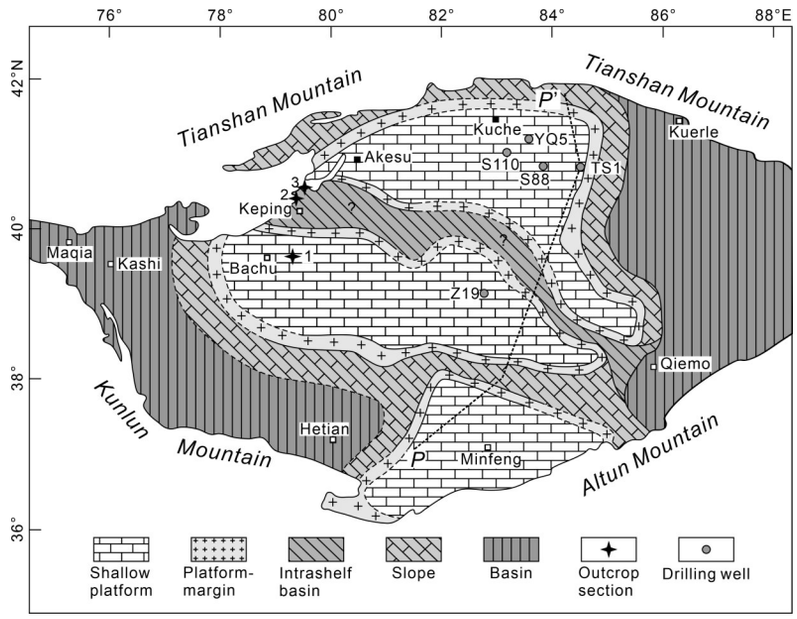

Figure 1. Paleogeography of the Tarim Basin during the Early–Middle Ordovician (modified from Guo et al., 2018b; Ren et al., 2015; Yan et al., 2010; Gu et al., 1994). The localities of section and drilling wells also are included. Section: 1. Dabantage (DBTG); 2. Keping (KP); 3. Tonggusibulong (TGSBL). The dashed line indicates the north-south profile (*P*–*P*') in Figure 2.

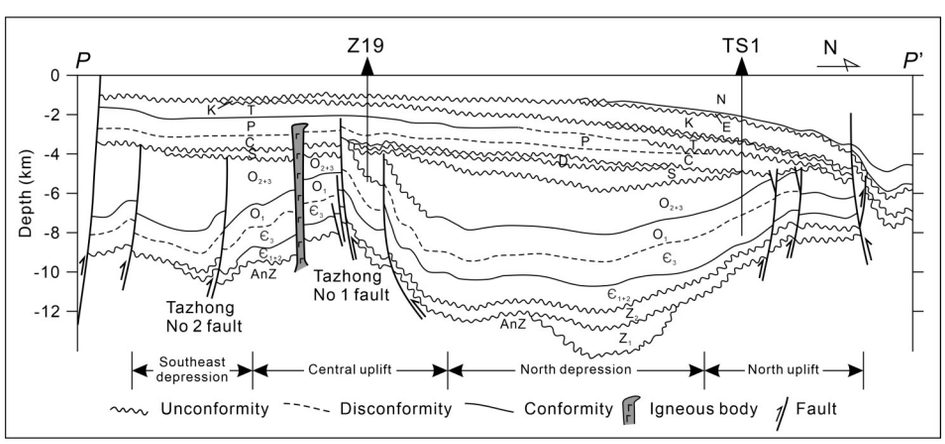

Figure 2. North-south profile (*P*–*P*' in Figure 1) showing the tecnostratigraphic framework across the Tarim Basin (modified from Zhu et al., 2015).

part is mainly composed of gray bioclastic-peloidal limestones interbedded with few dolomites of relatively open-marine subtidal environments (Guo C et al., 2018b; Guo F et al., 2010), in which burrow infills were represented by calcites. The burrow-associated carbonates are the focus of this study. The succeeding Yijianfang Formation, about 50 to 200 m thick and conformably overlying the Yingshan Formation, is characterized by gray micritic limestones in the lower part and by bioclastic limestones intercalated with micritic limestones in the upper part, respectively, pointing to an open-marine depositional environment (Zhang and Munnecke, 2016; Guo et al., 2010; Gu et al., 1994). The Qiaerbake (or Tumuxiuke) Formation (10 to 20 m), unconformably overlying the Yijianfang Formation, is represented by purple and reddish, argillaceous bioclastic limestones, indicating a condensed sequence of a quiet, deeper-water depositional environment (Zhang and Munnecke, 2016; Guo et al., 2010). The overlying Lianglitage Formation, 100 to 200 m thick, consists of dark gray micritic limestones in relatively restricted platform interior and reefal limestones at the high-energy platform margin, respectively (Zhang et al., 2017; Zhang and Munnecke, 2016).

2 METHODS

Detailed observations and descriptions were carried out on the outcrop section of Dabantage (DBTG) and core intervals from drilling wells penetrating the Yingshan Formation (Figure 1). During logging, representative samples were collected for petrographic and geochemical analyses. More than 100 thin sections of burrow-associated carbonates and their surrounding limestones within the Yingshan Formation were prepared for petrographic observation, some of which were stained with Alizarin-Red

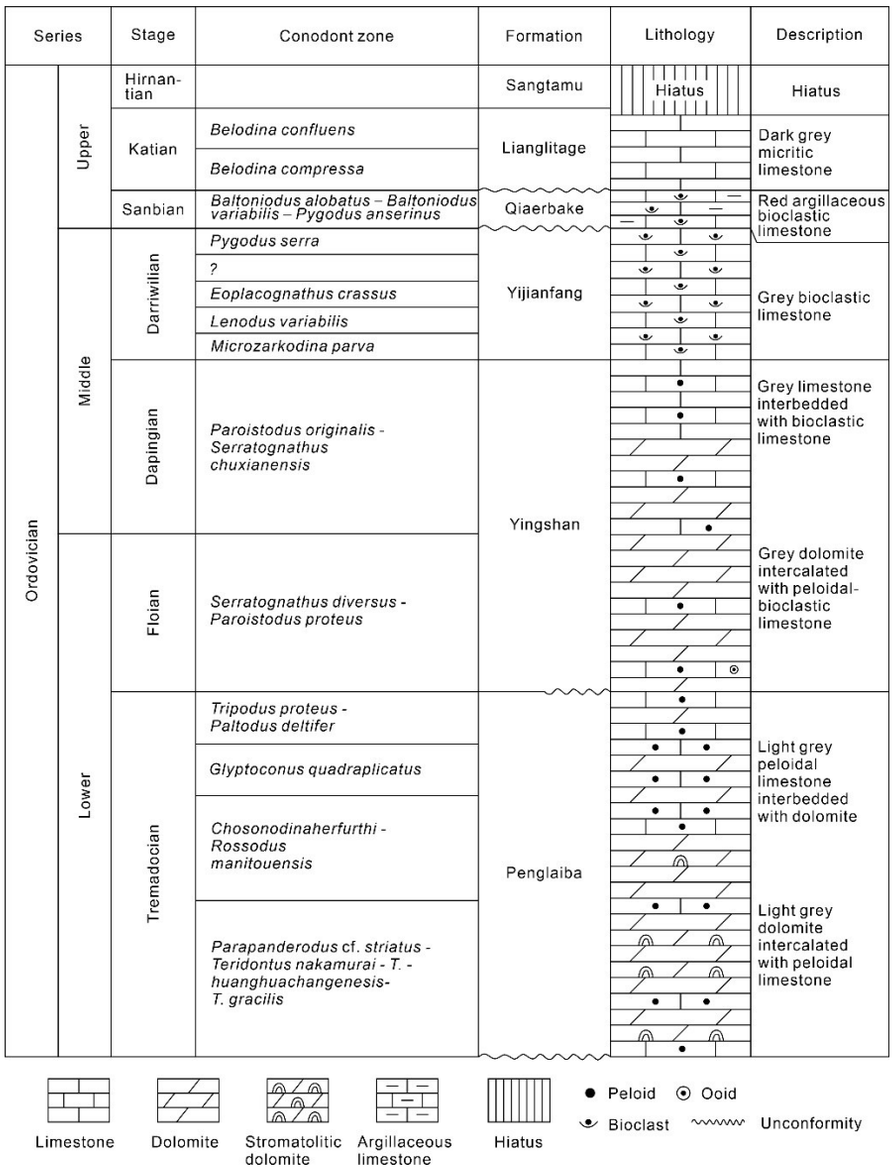

Figure 3. Lithostratigraphic units and main conodont zones of the Ordovician successions in the Tarim Basin, mainly based on data from Zhang and Munnecke (2016), Guo et al. (2010), Wang et al. (2007), and Zhao et al. (2006).

S and potassium ferricyanide to distinguish calcite from dolomite and ferroan carbonates from non-ferroan ones (Dickson, 1966). And some thin sections were also impregnated with pink epoxy, aiding in delineating porosity. These thin sections are examined using both conventional petrographic and cathodoluminescence microscopy. Cathodoluminescence microscopy was carried out on the RELION III stage at the Institute of Geology and Geophysics, Chinese Academy of Sciences (IGGCAS), under the average condition of a 5–8 kV gun potential and 300–500 mA beam current.

Thirty-nine samples for carbon and oxygen stable isotopic analyses were selected from representative outcrop and borehole core samples. The bulk powders were mechanically obtained using a dental drill (diameter < 1 mm) after a petrographic study. About 20 mg of sample powders of calcites and dolomites were reacted with anhydrous phosphoric acid (H_3PO_4) at 25 ºC for 24 h and 72 h, respectively (McCrea, 1950). For a mixture of calcite and dolomite (i.e., calcite and dolomite coexisting in burrows), CO_2 gases from these samples were extracted using the sequential chemical separation method of (Al-Aasm et al., 1990) in terms of different reaction rates of calcite and dolomite with the acid. The productive CO_2 gases were measured for carbon and oxygen isotopic ratios on a Finnigan MAT-253 mass spectrometer at IGGCAS. The oxygen isotopic values of calcites and dolomites were corrected using the fractionation factor of 1.009 88 (Swart et al., 1991) and 1.011 78 (Rosenbaum and Sheppard, 1986), respectively. The carbon ($\delta^{13}C$) and oxygen ($\delta^{18}O$) isotopic values were reported in per mille (‰) notation relative to the Vienna Pee Dee Belemnite (VPDB) standard. Calibrations of the $\delta^{13}C$ and $\delta^{18}O$ values were monitored daily isotope measurement through routine analysis of the International Standard NBS-19 sample ($\delta^{13}C$ = 1.95‰ VPDB; $\delta^{18}O$ = 2.20‰ VP-

DB). The precisions of both $\delta^{18}O$ and $\delta^{13}C$ values are better than 0.1‰. For the calculation of oxygen isotopic composition of parental fluids, the equilibrium oxygen isotope fractionation equations [$10^3\ln\alpha_{dolomite\text{-}fluid} = 3.2 \times 10^6 T^{-2} - 3.3$ and $10^3\ln\alpha_{calcite\text{-}fluid} = 2.78 \times 10^6 T^{-2} - 2.89$ of Land (1983) and $10^3\ln\alpha_{dolomite\text{-}fluid} = 2.73 \times 10^6 T^{-2} + 0.26$ of Vasconcelos et al. (2005)] was utilized for calcites and dolomites, respectively. The $\delta^{18}O$ conversion between VPDB and VSMOW scales was determined using the equation of $\delta^{18}O$ (VPDB) = 0.970 02 × $\delta^{18}O$ (VSMOW) – 29.98 according to (Coplen et al., 1983).

Eighteen newly-obtained samples and four samples from Guo et al. (2020, 2016) were selected for the measurement of strontium isotopic ($^{87}Sr/^{86}Sr$) ratios. Approximately 50–80 mg of sample powders were dissolved in 2.5 N HCl on the hotplate at 90 ºC. The strontium for analysis was extracted through the conventional cation exchange processes within a chromatographic column with 2 mlL of AG50Wx12 200–400 mesh cation exchange resin. The isotopic measurement of separated Sr was carried out on Finnigan MAT-262 mass spectrometer at IGGCAS. The results were normalized to the International Standard NBS-19 sample, the measured average $^{87}Sr/^{86}Sr$ ratio of which was 0.710 255 ± 0.000 012.

Microthermometry measurement of fluid inclusions was carried out on doubly polished thin sections (60 mm thick) on a Linkam THM600 heating-cooling stage at IGGCAS. The petrographic examination of fluid inclusions, including their occurrences within crystals and size consistency, and liquid/vapor ratios, was carefully performed to distinguish the primary or secondary origins (Goldstein, 2001). The accuracy of homogenization temperature (T_h) values is within 2.5 ºC.

3 OCCURRENCE AND PETROGRAPHY OF BURROW-ASSOCIATED CARBONATES

3.1 Occurrence of Burrow-Associated Carbonates

In most of the successions, burrow-associated carbonates are present as irregular patches of variable sizes, which are either perpendicular (subvertical) to bedding or irregular, forming distinctively colored mottles (or patches) in contrast to the ambient limestones (Figures 4 and 5a). The rock pattern resembles the dolomite mottles from the Middle Triassic ramp carbonates (Southern Hungary) (Török, 2000), the “gray pseudobreccias” from the Carboniferous of the Lake District (U. K.) (Horbury and Qing, 2004), the dolomite-mottled Ordovician Tyndall Limestone from Manitoba, Canada (Gingras et al., 2004b), the Type-3 dolomite observed within the Late Jurassic and earliest Cretaceous platform carbonates of the Jura Mountain (NW Switzerland, E France) (Rameil, 2008), and the dolomite-filled burrows within the Middle Devonian Lonely Bay Formation (Northwest Territories, Canada) (Corlett and Jones, 2012). Based on the mineralogical features, the burrow-associated carbonates are further divided into dolomite and calcite end members, whose distributional patterns generally are stratigraphically prone at different levels.

In the outcrop section where the Yingshan Formation is complete, the dolomite-dominated burrows are mainly concentrated in the lower part of the Yingshan Formation (Figure 6), which is represented by higher dolomite contents and was deposited in slightly restricted subtidal (i. e., lagoon) environments (Guo et al., 2018b). In contrast, the calcite-filled burrows commonly occur in the upper part of the formation, which is characterized by a remarkable decrease in dolomite content and was formed in restriction-improved subtidal environments (Guo et al., 2018b). In terms of the vertical stacking pattern of meter-scale, shallowing-upward cycles, both dolomite- and calcite-filled burrows are present in the lower–middle parts of cycles and locally extend upward into the capping peloidal packstone/grainstone of tempestite origin (Figure 5a). To a larger scale, the BADs are preferentially present in the regressive packages of third-order, even second-order depositional sequences in the lower part (Sq1–Sq2) of the Yingshan Formation (Figure 6), which represent deposits of a lowstand of long-term sea level (Guo et al., 2018b). In contrast, burrow-associated calcites (BACs) occur in the upper part (Sq4–Sq6) of the Yingshan Formation, which were formed in a transgression of long-term sea level (Guo et al., 2018b).

In the subsurface boreholes, the BADs were incompletely recovered in general, i. e., in the first and second core intervals of borehole YQ5 (Figure 7a; and see Figure 1 for location). The exact occurrence positions of these BADs at these levels, however, are difficult to be defined due to the incomplete penetration of the Yingshan Formation and its erosion of variable extents. Moreover, the BADs are also covered in the sixth to eighth core intervals of borehole Z19 in the central part of the basin (see Figure 1 for location), which are located in the upper part of the Yingshan Formation (Figure 7b). The host rocks of the sixth core interval of Well Z19 are mainly micritic limestones in composition, whereas those of the seventh and eighth core intervals were overwhelming dolomitized, which significantly improved the petroleum reservoir properties.

3.2 Petrography

Macroscopically, the dolomite-filled burrows are branched and 1 to 2 cm wide (Figure 4). In completely dolomitized intervals, the BADs have higher porosity and better reservoir properties than matrix dolomites (Figures 4c and 8a, 8g, 8h). The intercrystalline porosity of BADs are partially plugged by late calcite cements (Figures 4c and 8g, 8h). In partially dolomitized intervals, BADs do not show higher porosity than the matrix limestones that are mainly characterized by lime mudstone to bioclastic-peloidal wackestone/packstone in texture (Figures 4b, 4d and 8c). Of these, biofragments are mostly represented by minor trilobites, brachiopods, ostracods, and other undistinguished fossils. In some cases, the vertical and horizontal burrows are connected, some of which are constrained by low-amplitude stylolites (Figure 4d).

In thin section, most BAD crystals exhibit planar-s(e)

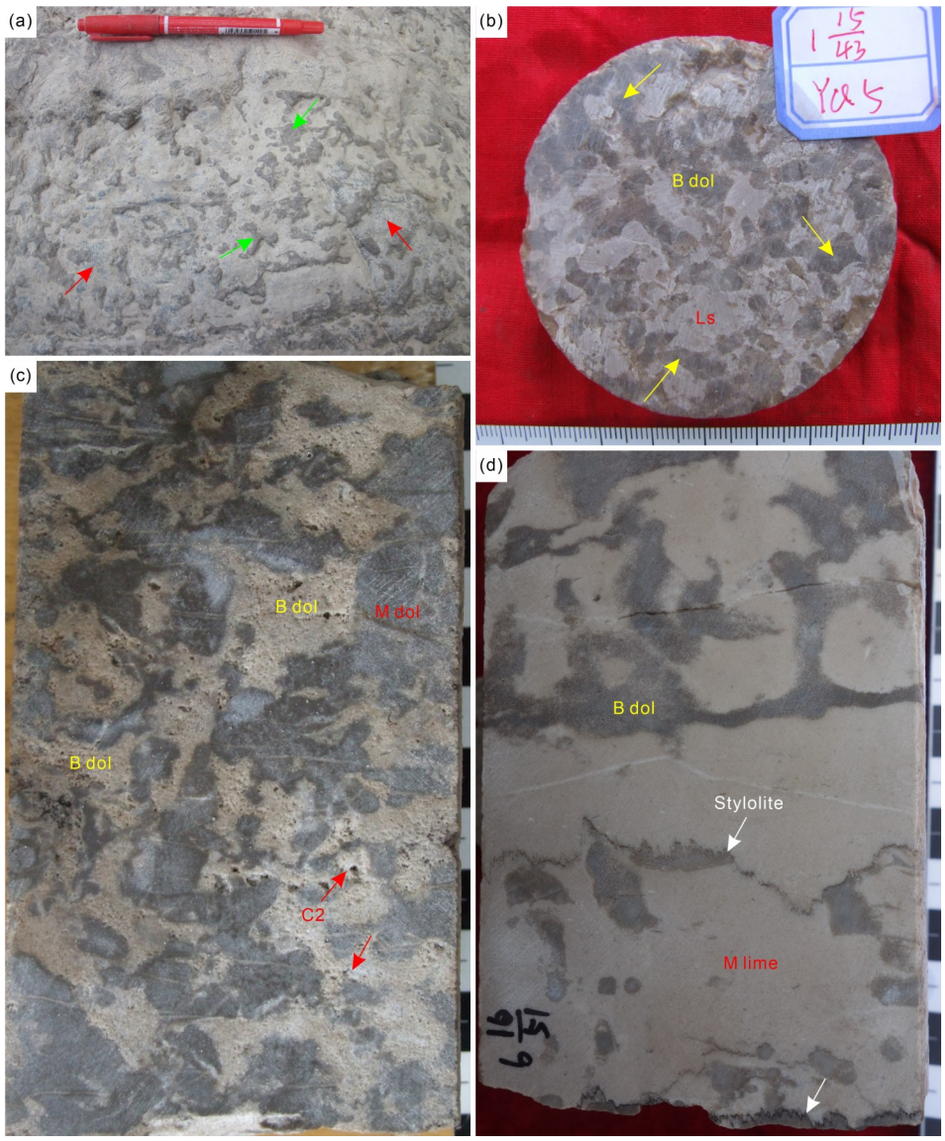

Figure 4. Burrow-associated dolomites (BADs) of Tarim Basin. (a) Field photo of BADs (green arrows) and matrix limestones (red arrows) in burrowed limestones (Guo et al., 2018b), showing a mottled appearance, DBTG. Pen for scale (14 cm long). (b) Core photo of BADs showing a dark gray color in contrast to light gray-colored matrix limestones in transverse section of drilling core. Well YQ5, 5 947.3 m deep. (c) Core photo of BADs (B-dol) showing a high porosity and a light gray color in contrast to dark gray-colored matrix dolomite (M-dol). Note the remaining pores partially occluded by calcites (C2). Scale (right) in cm. Well Z19, 5 549.7 m deep. (d) Core photo of BADs (B-dol) exhibiting vertical burrowing tubes and darker color compared to matrix limestones (M-lime). Note the serrated boundaries of dolomitized burrows that are defined by stylolites (white arrows), indicating burrows likely developed before or simultaneously with the formation of stylolites. Scale (right) in cm. Well Z19, 5 515.0 m deep.

textures and higher porosity compared to matrix dolomites of planar-s to nonplanar-a textures (Figure 8). The burrow-associated and matrix dolomite crystals both yield a cloudy center and clear rim texture (Figure 8). Under cathodoluminescence (CL), this texture shows a dull red luminescent center, followed by a non-luminescent zone and a subsequent bright red or orange luminescent rim (Figure 8b and 8d). In some cases, some BAD crystals display serrated surfaces (Figures 8a, 8g and 8h), and minor amounts of framboidal pyrite crystals are present within dolomitized burrow systems (Figure 8h). Locally, early calcite cements (C2) that partially to completely plug the porosity of BAD yield dull orange to non-luminescence under CL (Figure 8f). In places, some trilobite fragments are present around burrows and impinged by the growth of dolomite crystals within burrows. In addition, a few mm (or μm)-wide zones of scattered dolomite crystals (i. e., dolomitic halo; Gingras et al., 2004b) are present within matrix limestones and display a rapid decrease in number toward the surrounding calcitic matrix (Figure 8c). A similar phenomenon also was described by Rameil (2008) from the Late Jurassic and earliest Cretaceous platform carbonate of the Jura Mountain (NW Switzerland; E France).

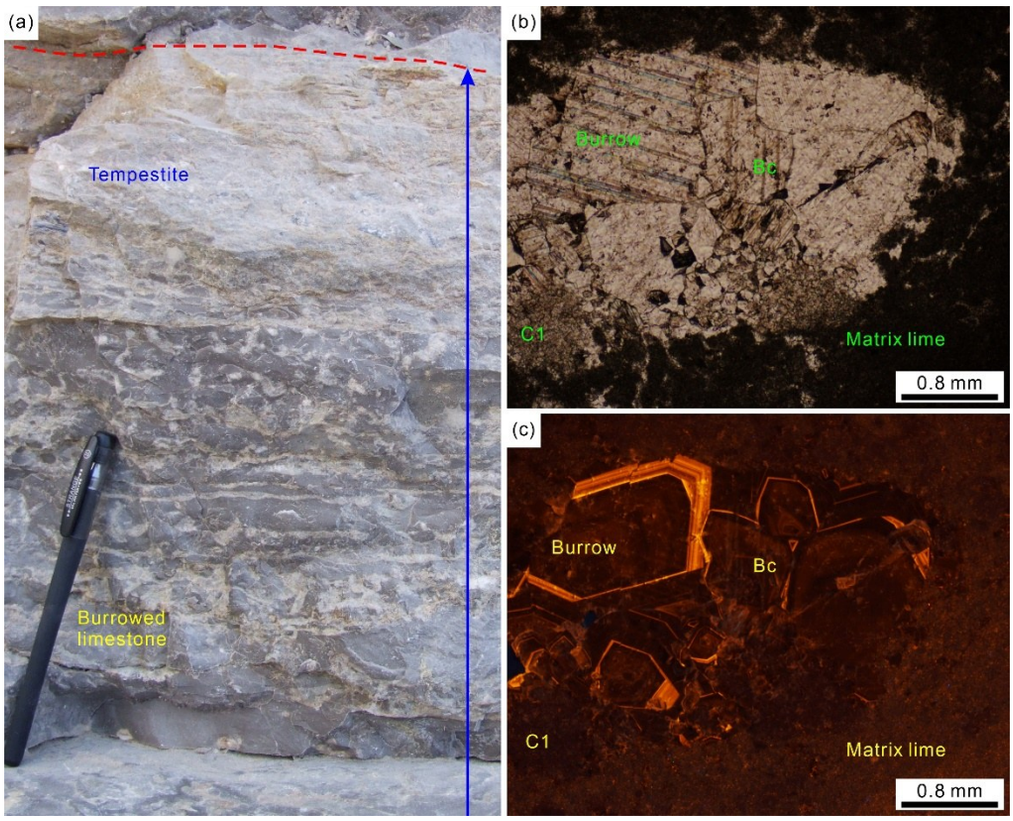

Figure 5. Burrow-associated calcite (BAC) in the outcrop of western Tarim Basin. (a) Field photo of burrowed limestone grading upward into tempestite, DBTG. The arrow line indicates a shallow-upward, meter-scale cycle and the dashed line denotes its upper boundary, DBTG. Pen for scale (15 cm long). (b), (c) Paired photomicrographs of BACs (C1) and blocky calcite cement (Bc) within a burrow of matrix limestones (Matrix lime), DBTG. (b) Plane-polarized light (PPL); (c) cathodoluminescence (CL).

In limestone-dominated intervals, burrow infills are mainly characterized by calcites in composition (Figure 5). Locally, burrow-associated infills are composed of backfilled calcitic material and later blocky calcitic sparites (Figure 5b), which display non-luminescence and a non-luminescent center followed by a zoned brighter rim, respectively (Figure 5c).

3.3 Paragenetic Sequence

The Lower – Middle Ordovician carbonate rocks of the Tarim Basin have experienced a complex diagenetic history since their deposition. Based on detailed field and core descriptions, conventional and cathodoluminescent microscopic studies, the paragenetic sequence of matrix dolomites, burrow-associated carbonates and other diagenetic minerals is summarized and illustrated in Figure 9. The early diagenetic stage (i.e., shallow burial) is roughly defined by the development of stylolites (Fabricius and Borre, 2007), and late one (i.e., deep burial) by the commence of fracturing (Jiang et al., 2016; Chen et al., 2004; Mountjoy and Halim-Dihardja, 1991).

In completely dolomitized intervals, most early diagenetic features (e.g., submarine cements) that were formed before burial or at shallow burial depth could have been usually masked or obliterated by dolomitization and/or late recrystallization processes (Machel, 1997; Mountjoy and Halim-Dihardja, 1991). Only in undolomitized or partially dolomitized carbonate rocks, can the relationship between matrix dolomites and early diagenetic phases (e.g., micrite and fibrous calcite cements) be identified, which will further be applied to constrain the relative timing of their development. Early diagenetic phases, such as fibrous and bladed calcite cements in inter-grain porosity in carbonate rocks, are commonly interpreted as being precipitated in submarine to shallow burial settings (Flügel, 2004; Tucker and Wright, 1990). In general, the development of low-amplitude stylolites is considered to start at depths of approximately 500 to 1 000 m (Fabricius and Borre, 2007). The burrow-associated calcareous silt/mud (C1) thus is interpreted to be formed simultaneously with or immediately after the burrow development. In contrast, the BADs were produced via the replacive dolomitization of burrow-associated calcareous material, thus post-dated the latter. Additionally, this type of dolomite is locally cut by the low-amplitude stylolites (Figure 4d), suggesting its formation, at least part of it, could be simultaneous with or pre-date the stylolitization (Fu et al., 2006; Mattes and Mountjoy, 1980). The matrix dolomite (Md) yields similar CL pattern to that of BADs (Figures 5d and 5f), but more curved crystal surfaces than the latter, indicating that the development of matrix dolomite should post-date BADs to some extent, partially overlapping with the BADs.

The dissolution of BADs and subsequent calcite ce-

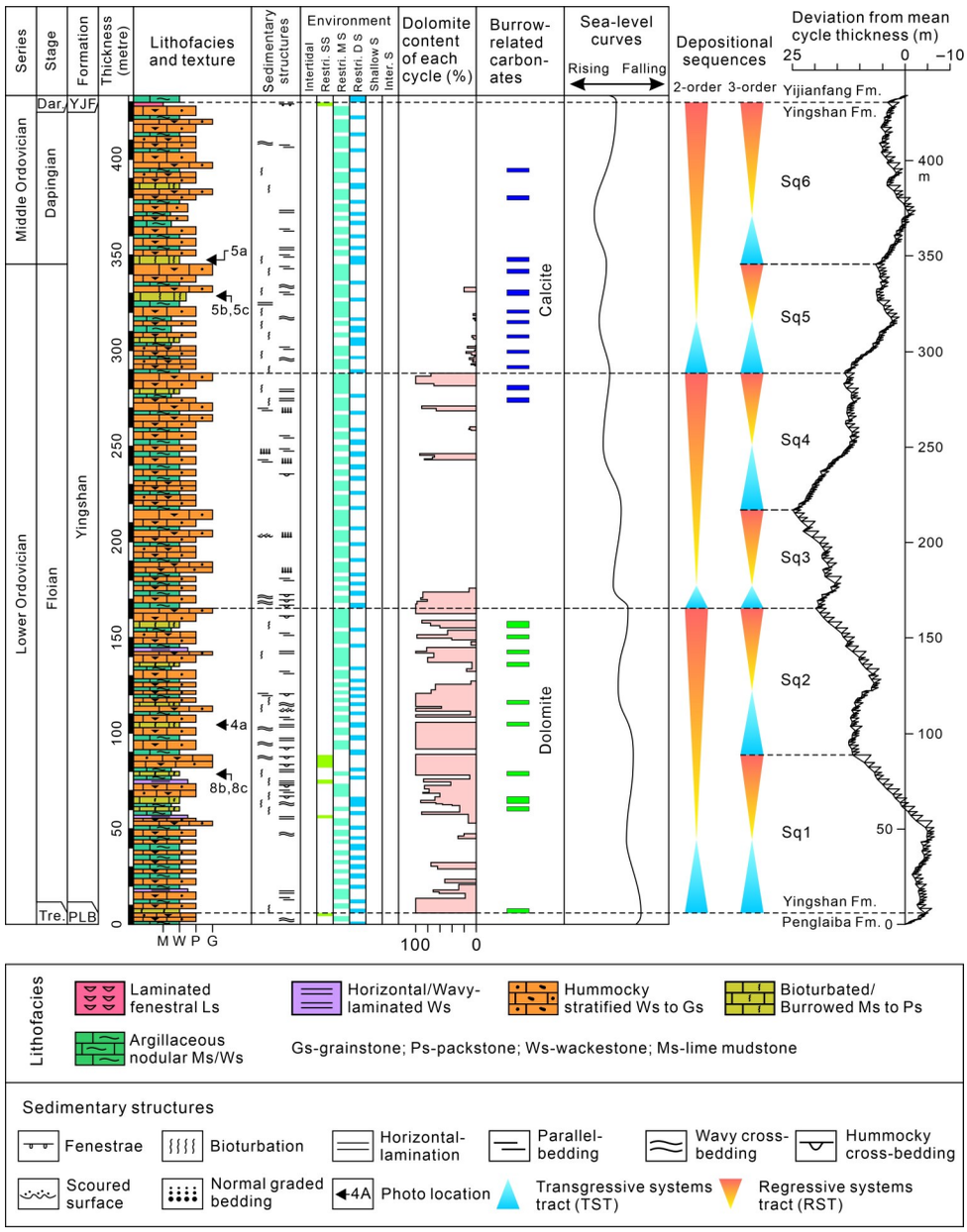

Figure 6. The vertical distributional pattern of burrow-associated carbonates within the Yingshan Formation at DBTG Section (modified after Guo et al., 2018b). The BADs and BACs are present in the lower and upper parts of the Yingshan Formation, respectively. Note the development of BADs and BACs are well correlated with the dolomite- and limestone-dominated intervals, respectively. Fm. Formation.

ments (C2) pre-dated hydrocarbon emplacement, as indicated by that oil/bitumen are not encountered between dolomite crystals and early calcite cements (C2) within burrows, but present in intercrystalline relict pores (Figures 8g and 8h). In addition, the fracturing event took place prior to hydrocarbon migration, as suggested by the presence of oil relicts (bitumen) within fractures (Figure 8h).

4 ISOTOPIC GEOCHEMISTRY AND FLUID INCLUSION MICROTHERMOMETRY

4.1 Oxygen and Carbon Isotopes

The $\delta^{13}C$ and $\delta^{18}O$ values of surrounding matrix limestones are compiled from the authors' previous study (Guo et al., 2020, 2016). They range widely from -2.3‰ to -0.9‰ VPDB (average -1.7‰; n = 21) and from -8.4‰ to -6.6‰ VPDB (average -7.6‰) (Table S1; Figure 10), respectively, generally falling within the estimated $\delta^{18}O$ range (-11.1‰ to -5.4‰ VPDB) and $\delta^{13}C$ range (-3.0‰ to 0 VPDB) for calcite precipitated from the Early – Middle Ordovician seawater (Shields et al., 2003; Veizer et al., 1999; Qing and Veizer, 1994).

In the outcrop of western Tarim Basin, the $\delta^{13}C$ values of BADs vary from -2.1‰ to -1.1‰ VPDB (average -1.8‰; n = 11) and $\delta^{18}O$ values from -8.0‰ to -4.9‰ VPDB (average -6.1‰) (Table S1; Figure 10). In the completely dolomitized intervals, the BADs from two samples have same $\delta^{13}C$ values of -1.8‰VPDB and $\delta^{18}O$ values

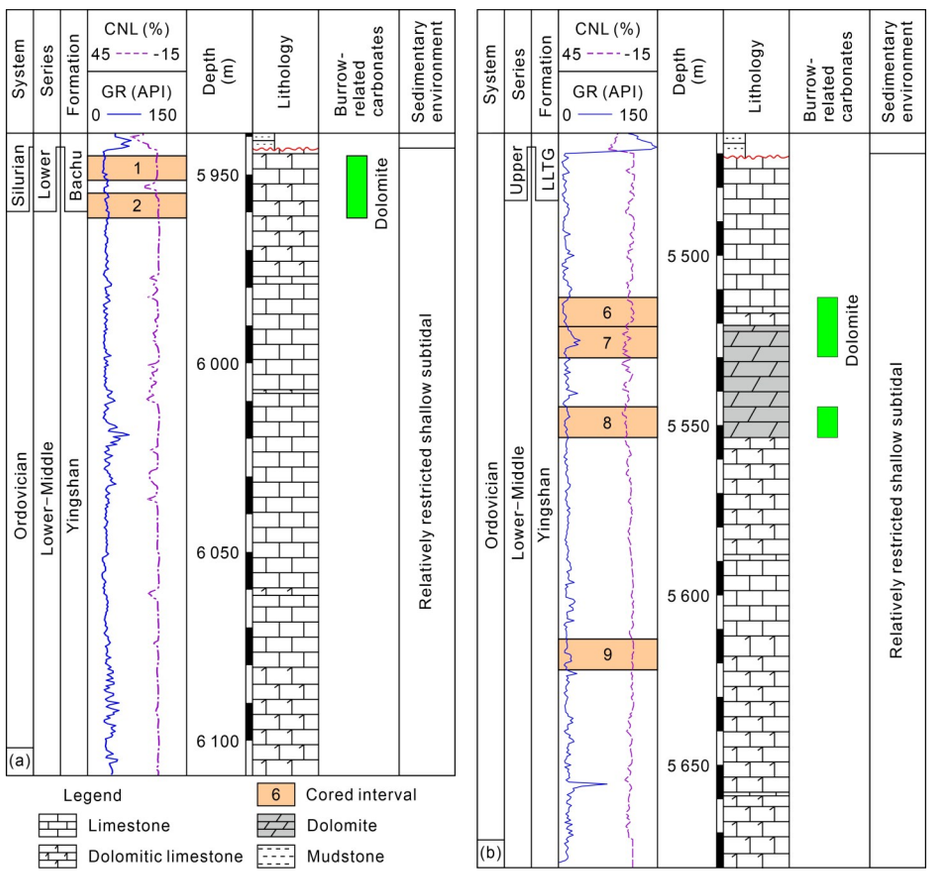

Figure 7. The vertical distributional pattern of BADs within the Yingshan Formation in the subsurface of northern (YQ5; (a)) and central (Z19; (b)) Tarim Basin. The BADs are difficult to be precisely placed within the Yingshan Formation in Well Z19 due to variable erosion and incomplete penetration.

from -8.3‰ to -8.1‰ VPDB (average -8.2‰), similar to those ($\delta^{13}C$: -2.1‰ to -1.8‰ VPDB, average -2.0‰; $\delta^{18}O$: -8.4‰ to -8.1‰ VPDB, average -8.3‰) of two surrounding matrix dolomites (Table S1; Figure 10).

In the subsurface of northern Tarim Basin, the $\delta^{13}C$ and $\delta^{18}O$ values of BADs from northern Tarim Basin vary from -2.0‰ to -1.6‰ VPDB (average -1.8‰; n = 6) and from -4.2‰ to -2.8‰ VPDB (average -3.7‰), respectively, which are slightly higher than those of their counterparts from the outcrop samples (Table S1; Figure 10). In the subsurface of central Tarim Basin, the $\delta^{13}C$ and $\delta^{18}O$ values of BADs range from -0.7‰ to -0.6‰ VPDB (average -0.7‰; n = 4) and from -9.7‰ to -7.1‰ VPDB (average -8.7‰), respectively. The $\delta^{13}C$ and $\delta^{18}O$ values of surrounding host dolomites vary from -1.0‰ to -0.6‰ VPDB (average -0.8‰; n = 4), and from -9.0‰ to -7.6‰ VPDB (average -8.3‰), respectively, which are consistent with those of corresponding BADs and matrix dolomites from the outcrop (Table S1; Figure 10).

In the calcite-dominated burrow intervals, the $\delta^{13}C$ and $\delta^{18}O$ values of BACs cluster between -1.6‰ and -1.1‰ VPDB (average -1.3‰; n = 4) and between -8.1‰ and -7.6‰ VPDB (average -7.9‰), respectively (Table S1; Figure 10).

The early-stage calcite cements (C2) have $\delta^{13}C$ values of -2.0‰ to -0.7‰ VPDB (average -1.0‰; n = 6), showing a large overlap with those of matrix limestones and dolomites, as well as BADs from the outcrop (Figure 10). Their $\delta^{18}O$ values range from -9.2‰ to -7.1‰ VPDB (average -8.2‰).

4.2 Strontium Isotope

Sr isotopic analysis was performed on eighteen samples analyzed for oxygen and carbon isotope and four samples from Guo et al. (2020, 2016) (Table S1; Figure 11). The $^{87}Sr/^{86}Sr$ ratios for matrix limestones of the Lower–Middle Ordovician Yingshan Formation vary from 0.709 018 to 0.709 170 (average 0.709 077; n = 4), comparable to estimated $^{87}Sr/^{86}Sr$ ratios (0.708 7–0.709 2) for the Early–Middle Ordovician marine limestones (Shields et al., 2003; Veizer et al., 1999; Burke et al., 1982).

In the outcrop section, the BADs yield $^{87}Sr/^{86}Sr$ ratios of 0.708 967 to 0.709 370 (average 0.709 111; n = 4). In completely dolomitized intervals, the matrix and burrow-associated dolomites have similar $^{87}Sr/^{86}Sr$ ratios, ranging from 0.709 024 to 0.709 156 (average 0.709 090; n = 2) and from 0.709 078 to 0.709 123 (average 0.709 101; n = 2), respectively.

In the subsurface of northern Tarim Basin, the $^{87}Sr/^{86}Sr$ ratios of BADs vary from 0.708 885 to 0.709 022 (average 0.708 952; n = 4), similar to those of their host limestones. In the subsurface of central Tarim Basin, the

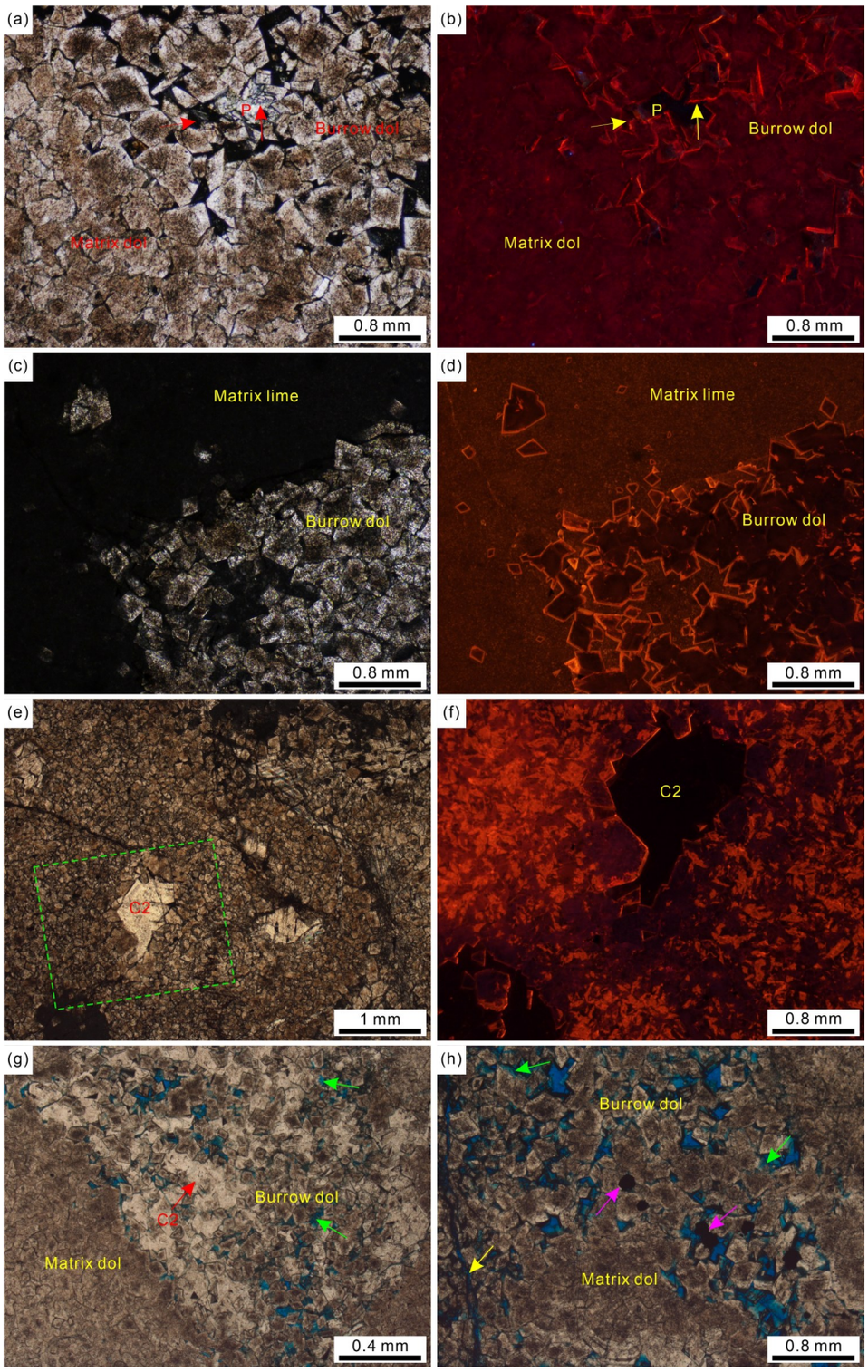

Figure 8. (a), (b) Paired photomicrographs of burrow-associated (Burrow dol) and matrix (Matrix dol) dolomites. Note the remaining pores (P) and serrated surfaces (arrows) of BAD crystals, DBTG. PPL (a) and CL (b). (c), (d) Paired photomicrographs of BADs (Burrow dol) and scattered euhedral dolomite crystals in matrix limestones. Well YQ5, 5 945.8 m deep. PPL (c) and CL (d). (e) Photomicrograph of the remaining pores in BADs that are cemented by early calcites (C2). Dashed The dashed rectangle denotes the field of F. Well YQ5, 5 948.8 m deep. PPL. (f) Photomicrograph of early-stage calcite cements (C2) showing non-luminescence. Well YQ5, 5 948.8 m deep. CL. (g) Photomicrograph of porous BADs (Burrow dol) with a planar-s(e) texture and densely packed matrix dolomite (Matrix dol) with a nonplanar-a texture. Note the corroded surfaces (green arrows) of dolomite crystals and subsequent calcite cements (C2) partially occluding the remaining pores. Well Z19, 5 549.9 m deep. PPL. (h) Photomicrograph of porous BADs (Burrow dol) and densely packed matrix dolomites (Matrix dol). Note the serrated surfaces (green arrows) of dolomite crystals and the presence of framboidal pyrites (pink arrows) and fractures (green arrow) impregnated with bitumen. Well Z19, 5 549.4 m deep. PPL.

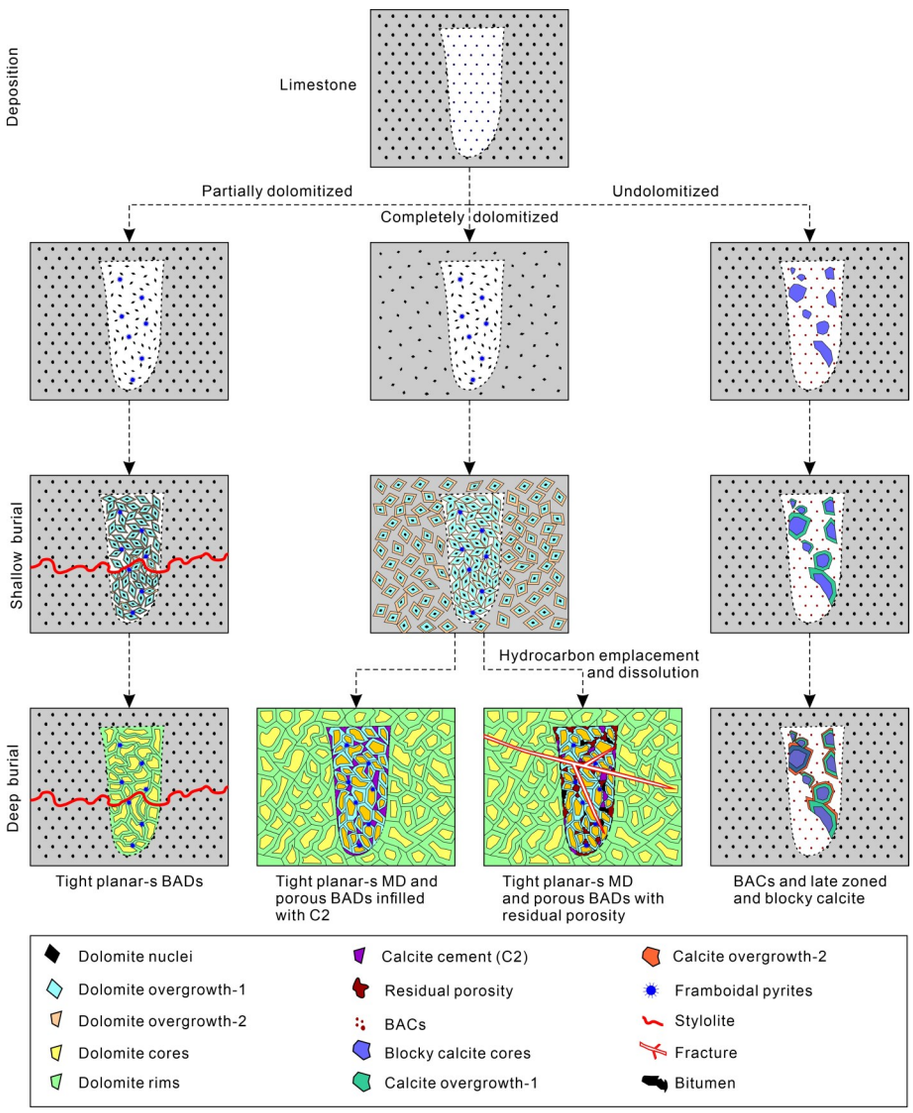

Figure 9. Schematic diagram illustrating the development of the diagenetic phases related to burrow-associated carbonates in the Lower–Middle Ordovician carbonate successions in the Tarim Basin based on detailed examination, conventional and cathodoluminescence microscopic analyses of field and drilling core samples.

BADs have comparable $^{87}Sr/^{86}Sr$ ratios from 0.709 012 to 0.709 123 (average 0.709 068; n = 2), also largely overlapping with those of coeval limestones (Figure 11). Additionally, the matrix dolomites yield $^{87}Sr/^{86}Sr$ ratios from 0.708 984 to 0.709 011 (average 0.708 998; n = 2), also comparable to their corresponding BADs.

In addition, the matrix limestones and BACs also share the similar $^{87}Sr/^{86}Sr$ ratios, varying from 0.709 018 4 to 0.709 103 (average 0.709 061; n = 2) and from 0.709 034 to 0.709 112 (average 0.709 073; n = 2), respectively.

4.3 Fluid Inclusion Microthermometry

Microthermometric measurements of two-phase (liquid and vapor) primary aqueous fluid inclusions assemblages (FIAs) from BADs and early-stage calcite cements in central Tarim Basin were performed to measure the homogenization temperatures (T_h), which represents minimum estimates of entrapment temperatures of fluids. Fluid inclusions are small (commonly 3 – 8 μm across), and have elongate or irregular shapes, with vapor/fluid ratios of 5%–10% (Figure 12). The T_h values in the individual FIAs are relatively consistent, indicating a minimum effect of re-equilibration on T_h (Goldstein, 2001). The BAD crystals in central Tarim Basin yield T_h values of 73.6 – 85.7 ºC (average 80.1 ºC) (Table 1; Figure 13). The early-stage calcite cement has T_h values varying from 77.7 – 93.4 ºC (average 84.9 ºC) (Table 1; Figure 13).

5 INTERPRETATION AND DISCUSSION

5.1 Origin of Burrow-Associated Carbonates

The origin of mottled dolomites is a controversial topic (e. g., Purser et al., 1994; Tucker and Wright, 1990; Land, 1985). Several mechanisms have been put forward to elucidate the origin of mottled dolomites, including fracture-controlled hydrothermal dolomitization (e. g., Chen et al., 2004; Malone et al., 1996; Mountjoy and Halim-Dihardja, 1991), dolomitization of karstic breccias

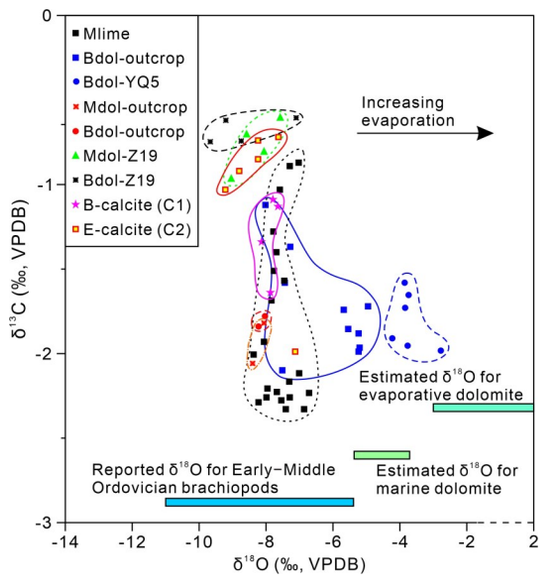

Figure 10. Cross-plot of $\delta^{13}C$ and $\delta^{18}O$ values of BADs, BACs, and surrounding matrix carbonates. The estimated $\delta^{18}O$ values for dolomites of coeval seawater origin were calculated based on the $\delta^{18}O$ values of micritic limestones and $\Delta^{18}O_{dol\text{-}cal}$ (+3‰; Budd, 1997). The $\delta^{18}O$ values of Early–Middle Ordovician brachiopods (Shields et al., 2003; Veizer et al., 1999; Qing and Veizer, 1994) and evaporative dolomites (Montañez and Read, 1992) are also given for comparison. Abbreviations: Mlime. Matrix limestones; Mdol. matrix dolomites; Bdol. burrow-associated dolomites (BADs); B-calcites (C1). burrow-associated calcites (BACs); E-calcite (C2). early-stage calcite cements.

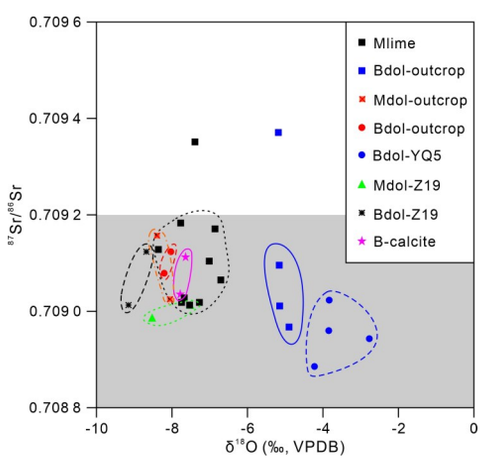

Figure 11. Cross-plot of $^{87}Sr/^{86}Sr$ and $\delta^{18}O$ values of matrix and burrow-associated carbonates in the Tarim Basin. The gray area denotes the $^{87}Sr/^{86}Sr$ ratio ranges of the Early–Middle Ordovician seawater (Shields et al., 2003; Veizer et al., 1999; Burke et al., 1982). Most of $^{87}Sr/^{86}Sr$ ratios of matrix and burrow-associated carbonates are comparable to those expected for carbonates precipitated from coeval seawater. Note no apparent trend of increasing Sr isotopic ratios with decreasing oxygen isotopic ratios. See Figure 10 for abbreviations.

(e.g., Kupecz and Land, 1991; Kerans, 1988), and burrow-associated, selective dolomitization (e.g., Corlett and Jones, 2012; Rameil, 2008; Gingras et al., 2004a; Horbury and Qing, 2004; Török, 2000). Previous researches revealed that parts of the Tarim Basin have been subject to intense hydrothermal activities triggered by faulting/fracturing and intrusive magmatism (Dong et al., 2013; Zhu et al., 2010; Jin et al., 2006). The fracture-controlled hydrothermal dolomitization model, however, is unlikely to be responsible for the formation of BADs within the Yingshan Formation since few large-scale faults/fractures and hydrothermal minerals (i.e., fluorite, barite, and quartz; e.g., Guo et al., 2016; Jia et al., 2016; Dong et al. 2013) are not encountered within burrow-bearing successions. Although large-scale unconformity-related karstic reservoirs are ubiquitously present within the Ordovician carbonate rocks of the Tarim Basin (Lin et al., 2013; Jia and Wei, 2002), the possibility of dolomitization of karstic breccias can be also ruled out due to that the uplift-related subaerial weathering features also did not occur within burrow-occurring successions. Selective dolomitization is considered to be the most reasonable formation mechanism responsible for the development of the mottled BADs in the Yingshan Formation. This interpretation is also supported by the fact that the studied Yingshan Formation was deposited in a storm-influenced carbonate platform interior (i.e., lagoon) (Guo et al., 2018b). This depositional environment is suitable for some endobenthic organisms to inhabit or burrow down into sediments below the surface for dwelling, foraging, and feeding, creating burrows of complex ichnofabrics and morphologies with backfilled disputed lime muds/silts (Donovan, 1994; Ekdale et al., 1984). These burrow-infills could have been either selectively dolomitized or remained carbonaceous, both of which are commonly mottled in color and composition (Figures 4, 5, and 8), and enhanced in later diagenetic processes.

5.1.1 Origin of burrow-associated dolomites

5.1.1.1 Petrographic implications The paleogeographic setting (i.e., lagoon) of the Yingshan Formation generally favored the early dolomitization (e.g., Guo et al., 2017; Vinci et al., 2017; Qing et al., 2001; Sun, 1994). The preferential occurrence of BADs in the regressive packages of third-order, even second-order depositional sequences in the lower part (Sq1–Sq2) of the Yingshan Formation (Figure 6) denotes that their formation was dictated by long-term sea-level fluctuations. On a small scale, it is noted that the BADs preferentially occurred in the lower–middle part of meter-scale depositional cycles, indicating that their formation (i.e., selective dolomitization) was intimately associated with high-frequency (fourth to fifth-order) sea-level fluctuations (e.g., Vinci et al., 2017; Sun, 1994). In contrast to western Tarim Basin, the BADs in the subsurface of northern and central Tarim Basin took place in the upper part of the Yingshan Formation (Figure 7), which differs from the distributional pattern of BADs in the outcrop. This discrepancy indicates the BAD development was likely controlled by the combination of sea-level variations of variable orders and paleo-topography (or depositional environments).

Table 1 Fluid inclusion data of BADs and early-stage calcite cements in central Tarim Basin

Sample	Mineral type	No. of inclusions	T_h (ºC)		
			Minimum	Maximum	Average
Z19-14	Matrix dolomites	3	73.6	82.3	77.3
Z19-16	Matrix dolomites	3	79.3	85.7	83.5
Z19-10	Early-stage calcite cements	4	85.5	93.4	89.5
Z19-14	Early-stage calcite cements	6	81	89.5	86.2
Z19-16	Early-stage calcite cements	5	77.7	82.5	79.8

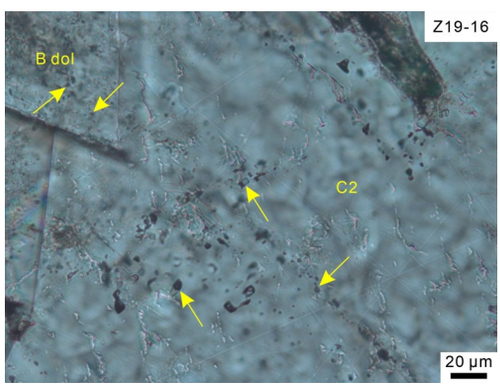

Figure 12. Photomicrograph of fluid inclusion (arrows) in BADs (B-dol) and early-stage calcite cements (C2) in central Tarim Basin.

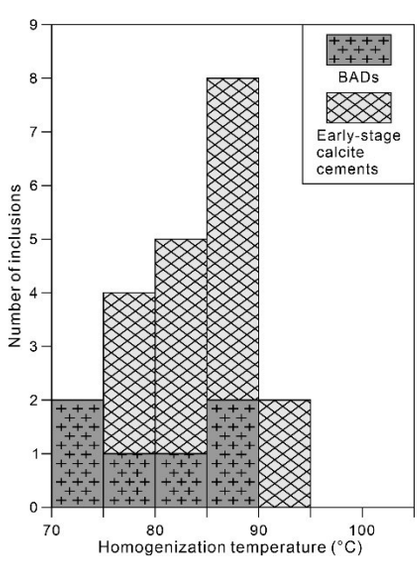

Figure 13. Histogram showing distributions of fluid inclusion homogenization temperatures (T_h) in BADs and early-stage calcite cements in central Tarim Basin.

Although both burrow infills and surrounding host limestones are locally replaced completely by dolomites (Figures 4c and 8a, 8f, 8g, 8h), most of the host limestones escaped from dolomitization (Figures 4a, 4b, 4d, and 8c), denoting that the dolomitizing fluids were slightly less supersaturated in terms of dolomites or not sufficient for complete dolomitization (e. g., Warren, 2000; Sibley and Gregg, 1987). In some cases, the BADs were cut by stylolites or dissolution seams (Figure 4b), suggesting that these dolomites could have been formed before or concurrently with the development of stylolites. It has been revealed that the production of stylolites in carbonate rocks requires a minimal burial depth of approximately 500 m (Fabricius and Borre, 2007; Mountjoy et al., 1999). Thus, the dolomitization of the burrow infills could persist into shallow burial depths of about 500 to 1 000 m during the Late Ordovician (Figure 14). This interpretation is also endorsed by the dominance of subhedral to euhedral crystals of BADs (Figure 8), pointing to their formation at temperatures lower than the critical roughening temperature for dolomites (50–60 ºC; Sibley and Gregg, 1987; Gregg and Sibley, 1984). Assuming an annual average surface temperature of 20 °C and a normal geothermal gradient of 30 °C/km for the Lower–Middle Ordovician carbonate successions in the Tarim Basin (e. g., Guo et al., 2017; Qiu et al., 2012; Li et al., 2005), the burial depth of around 1 000 m during the Late Ordovician (Figure 4) could produce the temperatures of 50–60 ºC, reconciling the formation of BADs in such a diagenetic setting.

5.1.1.2 Geochemical constraints The $\delta^{13}C$ features of dolomites generally inherit from precursor limestones and mirror the $\delta^{13}C$ characteristics of parental limestones due to little isotopic fractionation of $^{13}C/^{12}C$ with temperature (Warren, 2000; Budd, 1997; Banner and Hanson, 1990; Land, 1980). In addition, the $^{87}Sr/^{86}Sr$ signatures of carbonate minerals also record the Sr-isotopic composition of their parental fluids because of negligible Sr-isotopic fractionation during carbonate precipitation (Banner, 1995; Tucker and Wright, 1990). However, there is an important problem when comparing the isotopic compositions of dolomites with those of limestones because the relationship between $\delta^{18}O_{fluid}$ and $\delta^{18}O_{dolomite}$ is still not defined (Warren, 2000; Budd, 1997; Tucker and Wright, 1990; Land, 1980). Previous studies suggested that the oxygen isotopic fractionation between dolomites and calcites ($\Delta^{18}O_{dol\text{-}cal} = \delta^{18}O_{dolomite} - \delta^{18}O_{calcite}$ on the VPDB scale) varies from 2‰ to 6‰ (see review in Budd, 1997). A mean value of +3‰ is taken as $\Delta^{18}O_{dol\text{-}cal}$ representing the fractionation between dolomite and calcite, which is widely accepted (e. g., Rameil, 2008; Budd, 1997; Land, 1985, 1983). The $\delta^{13}C$ and $\delta^{18}O$ values of surrounding matrix limestones from the outcrop (-2.3‰ to -0.9‰ VPDB and -8.4‰ to -7.1‰ VPDB, respectively) and northern Tarim Basin (-2.3‰ to -2.1‰ VPDB and -7.2 to -6.6‰ VPDB, respectively) are comparable to those of the published $\delta^{13}C$ (-3.0‰ to 0 VPDB) and $\delta^{18}O$ (-5.4‰ to -11.1‰ VPDB) values for contemporaneous brachiopods (Figure

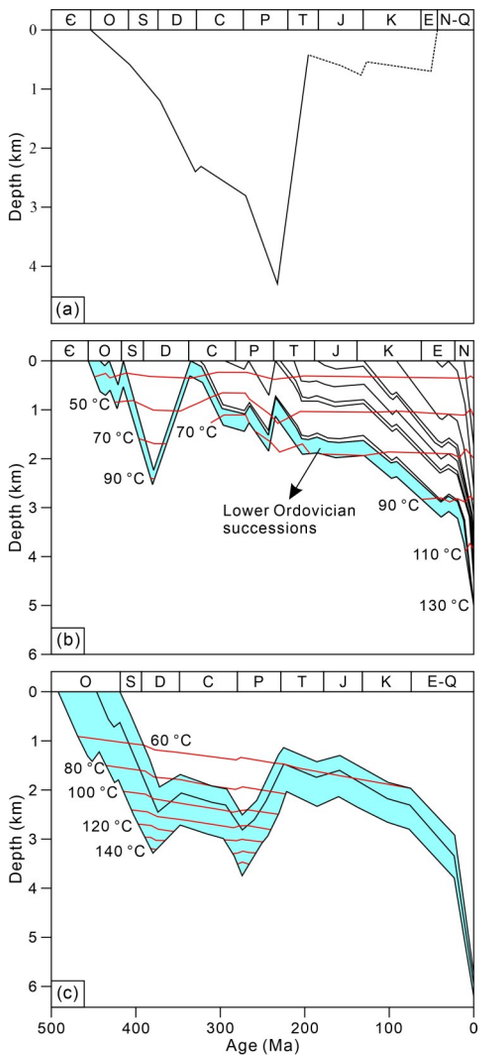

Figure 14. Burial history of the Lower–Middle Ordovician carbonate successions in the Tarim Basin, represent western, northern and central Tarim Basin, respectively. (a) Modified from Ye (1994); (b) based on wells S75 and S15 (modified from Guo et al. (2016), Li et al. (2011)); (c) based on wells TZ1 and ZS5 (modified from Qiu et al. (2012)).

10) (Shields et al., 2003; Veizer et al., 1999; Qing and Veizer, 1994), indicating that matrix limestones did not experience intensive diagenetic alteration. This interpretation is also supported by the $^{87}Sr/^{86}Sr$ ratios of matrix limestones that mostly fall within the estimated $^{87}Sr/^{86}Sr$ range of calcites precipitated from the coeval seawater (Figure 11) (Shields et al., 2003; Veizer et al., 1999; Burke et al., 1982). Thus, the matrix limestones are considered to well preserve the geochemical signatures of the Early–Middle Ordovician seawater and can be applied as a representative for the contemporaneous seawater.

Overall, the $\delta^{13}C$ values of the BADs from the outcrop (-2.1‰ to -1.1‰ VPDB), northern (-2.0‰ to -1.6‰ VPDB), and central (-0.7‰ to -0.6‰ VPDB) Tarim Basin are consistent with those of matrix limestones, and cluster within the reported $\delta^{13}C$ values (-3.0‰ to 0 VPDB) of coeval seawater (Figure 10) (He et al., 2025; Shields et al., 2003; Veizer et al., 1999; Qing and Veizer, 1994), also reflecting that the carbon isotopic signature of BADs was derived from precursor limestones (Ding et al., 2020; Fu et al., 2006; Gregg and Shelton, 1990). Most of the $\delta^{18}O$ values of BADs from the outcrop (-8.0‰ to -4.9‰ VPDB) and northern Tarim Basin (-4.2‰ to -2.8‰ VPDB) fall within the estimated $\delta^{18}O$ values (-5.4‰ to -3.6‰ VPDB) of coeval seawater dolomite based on the $\Delta^{18}O_{dol\text{-}cal}$ (+3‰) and the $\delta^{18}O$ values of matrix limestones, indicating the dolomitizing fluids responsible for BAD precipitation were also derived from contemporaneous seawater (e.g., Budd, 1997; Land, 1980). The $\delta^{18}O$ values (-9.7‰ to -7.1‰ VPDB) of BADs from central Tarim Basin are comparable to those (-9.0‰ to -7.6‰ VPDB) of the surrounding matrix dolomite but more negative than those of their counterparts from the outcrop and northern part of the basin, indicating the former could have been subject to intense recrystallization or later diagenetic alteration during deeper burial (e.g.,Machel, 2004, 1997). Applying the calcite-fluid oxygen-isotope fractionation equation of Land (1983), and assuming the surface temperatures of 20 to 25 ºC (e.g., Guo et al., 2020, 2016; Jiang et al., 2016), the $\delta^{18}O$ values of the Early–Middle Ordovician seawater vary from -7.4‰ to -4.7‰ VSMOW (Figure 15). Applying the dolomite-fluid oxygen-isotope fractionation equation of Vasconcelos et al. (2005) for low-temperature dolomites, and assuming the precipitation temperatures of 30 to 50 ºC (i.e., slightly higher than surface temperatures and lower than the critical roughening temperature of 50–60 ºC (Sibley and Gregg, 1987; Gregg and Sibley, 1984) for dolomites at shallow depth (e.g., Jiang et al., 2016), the $\delta^{18}O$ values of the parental fluids, from which the BADs in the outcrop of western Tarim Basin was precipitated, range from -7.5‰ to -0.9‰ VSMOW (Figure 15). In contrast, the $\delta^{18}O$ values of dolomitizing fluids for the precipitation of BADs in northern and central Tarim Basin vary from -3.8‰ to +1.3‰ VSMOW and from -2.6‰ to +1.8‰ VSMOW (Figure 15), respectively, based on the estimated precipitation temperatures (30 to 50 ºC) for BADs from the northern part and the T_h values (73.6–85.7 ºC) for BADs from the central part. The calculated $\delta^{18}O$ values of the dolomitization fluids for BAD precipitation in the outcrop of western Tarim Basin are largely overlapped with but higher than those $\delta^{18}O$ values of coeval seawater calculated from micritic limestones, implying the dolomitizing fluids responsible for BAD precipitation are mainly characterized by slightly evaporated seawater (i.e., mesosaline seawater) (e.g., Guo et al., 2020, 2017, 2016; Qing et al., 2001; Jones et al., 2000). In addition, the calculated $\delta^{18}O$ values of the dolomitizing fluids within burrows in northern and central Tarim Basin are also largely overlapped with the calculated $\delta^{18}O$ values for BADs in western Tarim Basin but are more positive than $\delta^{18}O$ values of coeval seawater (Figure 15), suggesting these dolomites were precipitated from more ^{18}O-enriched fluids that were likely characterized by more intensively evaporated seawater. Although the recrystallization within ^{18}O-enriched fluids as a result of enhanced

water-rock interaction can lead to higher $\delta^{18}O$ values of resultant dolomites, the absence of positive covariance between $\delta^{18}O$ and $^{87}Sr/^{86}Sr$ (Figure 11) rules out this possibility. Moreover, the large overlap of $^{87}Sr/^{86}Sr$ ratios of BADs with those of micritic limestones and coeval seawater (Figure 11) also suggests that the dolomitizing fluids could have derived from the contemporaneous seawater. Based on the stable isotopes, major and trace elements, previous studies also suggested that the dolomites with similar $\delta^{13}C$ and $^{87}Sr/^{86}Sr$ signatures to the BADs could be formed from evaporated seawater or seawater-derived fluids (e.g.,Hu et al., 2019, 2011; Zhu et al., 2010; Shao et al., 2002). This also supports the conclusion that the BADs should be formed from variably-evaporated coeval seawater.

5.1.1.3 Formation mechanism of BADs The BAD formation have been interpreted as linking to anoxic conditions (Meister et al., 2007; Mazzullo, 2000; Baker and Burns, 1985), the presence of sulfate-reducing bacteria (SRB) (Wright and Wacey, 2005; van Lith et al., 2003), the occurrence of marine-sourced organic matter (Corlett and Jones, 2012; Bontognali et al., 2010; Slaughter and Hill, 1991), and a sufficient supply of magnesium (Machel, 2004; Warren, 2000; Morrow, 1982). Recently, Corlett and Jones (2012) have documented petrographic and geochemical contrasts between dolomites and calcites both infilling burrows in the Middle Devonian Lonely Bay Formation, Northwest Territories, Canada. The authors concluded that the early selective dolomitization of burrow infills could be operative when the specific four prerequisites mentioned above were obtained. The Yingshan Formation in the Tarim Basin was commonly developed solely in marine depositional environments (Guo C et al., 2018b; Lin et al., 2013; Guo F et al., 2010; Feng et al., 2007). In such a circumstance, the supply of Mg^{2+} sourced from normal seawater or slightly evaporation-modified seawater, the occurrence of sulfate-reducing bacteria and marine-derived organic material, and the anoxic conditions could be obtained (e.g., Schulz and Zabel, 2006; Haley et al., 2004). The burrow infills in the Yingshan Formation, however, are not exclusively characterized by dolomite in composition (Figure 6). In addition, the presence of BADs corresponds to relatively low sea-level conditions, whereas the development of BACs is related to relatively high sea-level conditions. These suggest that other factors (i.e., Mg^{2+} concentration) could have also controlled the precipitation of burrow-associated carbonates (e.g., Hardie, 1987; Folk and Land, 1975).

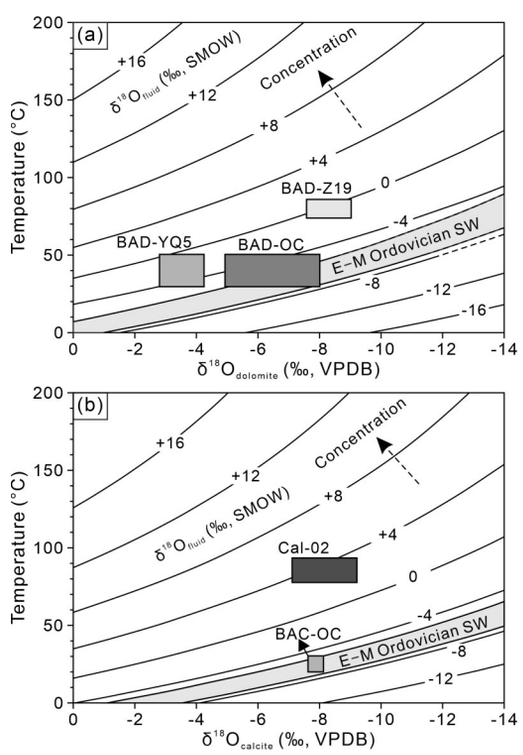

Figure 15. Cross-plot of $\delta^{18}O$ versus temperatures of different types of BADs and early-stage calcite cements. For BADs (a), the dolomite-fluid equation: $10^3 \ln\alpha_{dolomite\text{-}fluid} = 2.73 \times 10^6\ T^{-2} + 0.26$ (Vasconcelos et al., 2005) and $10^3 \ln\alpha_{dolomite\text{-}fluid} = 3.2 \times 10^6\ T^{-2} - 3.3$ (Land, 1983) was applied for low- (< 50 °C) and high-temperature (> 50 °C) dolomites, respectively. For calcite phase (b), the calcite-fluid equation: $10^3 \ln\alpha_{calcite\text{-}fluid} = 2.78 \times 10^6\ T^{-2} - 2.89$ (Land, 1983) was used. Note the progressive increasing trend in ^{18}O enrichment of parental fluids from the western (outcrop; OC) through northern (YQ5) to central (Z19) parts of the Tarim Basin. Abbreviations: BAD. Burrow-associated dolomites; BAC. burrow-associated calcites; Cal-02. early-stage calcite cements; E–M Ordovician SW. Early–Middle Ordovician seawater.

A conceptual model was invoked to explain the BAD development (Figure 16). During relatively high sea level, water circulation between the lagoon and open ocean was comparatively excellent. The lagoon was likely occupied by seawater with a normal salinity, in which massive burrows were probably formed by burrowing organisms and filled with normal seawater of normal salinity (Figure 16a). Meanwhile, reflux dolomitization may only occur in peritidal to shallow lagoonal settings near the coastline when hypersaline brines percolated through the underlying sediments due to a density difference between evaporated seawater and the underlying pore water caused by an elevation in salinity as a result of evaporation (e.g., Jiang et al., 2013; Qing et al., 2001; Jones et al., 2000; Adams and Rhodes, 1960). Under conditions of long-term low sea-level, the water circulation of the lagoon to open ocean became progressively limited due to the barrier effect of high-energy platform rims during relatively low sea-level, leading to the occupation of comparatively evaporated (i.e., mesosaline to penesaline) seawater with relatively elevated concentration of magnesium ions (Mg^{2+})in lagoonal environments (Figure 16b). In such a circumstance, both fine-grained sediments and burrow-infills in lagoonal environments could have been completely dolomitized by the reflux of these modified fluids (Figures 4c and 8a, 8g, 8h) (Kaufman, 1994; Sun, 1994). In the case of relatively low concentration and limited supply of Mg^{2+} due to the comparatively weaker barrier effect of high-energy platform rims, only were burrow infill-

ings completely dolomitized, leaving surrounding matrix limestones unaffected (Figures 4a, 4b, 4d, 8c, 8e). In contrast, under conditions of long-term high sea-level, neither burrow-infills nor matrix rocks were not affected by the dolomitization process even during short-term relatively low sea level (Figures 5 and 16c). This is likely attributed to comparatively good water circulation between the lagoon and open ocean due to the progressively weakened barrier effect of high-energy platform rims, leading to the occupation of nearly normal seawater in lagoonal environments (Figure 16c).

Burrowing organisms notably alter the properties of sediment substrates in various ways, including biomechanical and biochemical modification (Gingras et al., 2004b; Bromley, 1996). The physical processes of burrowing can cause a reduction in grain size (Chow and Longstaffe, 1995), which provides larger surface areas to interact with dolomitizing fluids and provides a significant number of nucleation sites per given volume for dolomite crystals (Gingras et al., 2004b; Sibley and Gregg, 1987). Open burrows or burrows filled with backfilled loose lime materials served as potential open conduits to the sediment-water interface and also to the fluids contributing to the formation of burrow-associated carbonates. More-

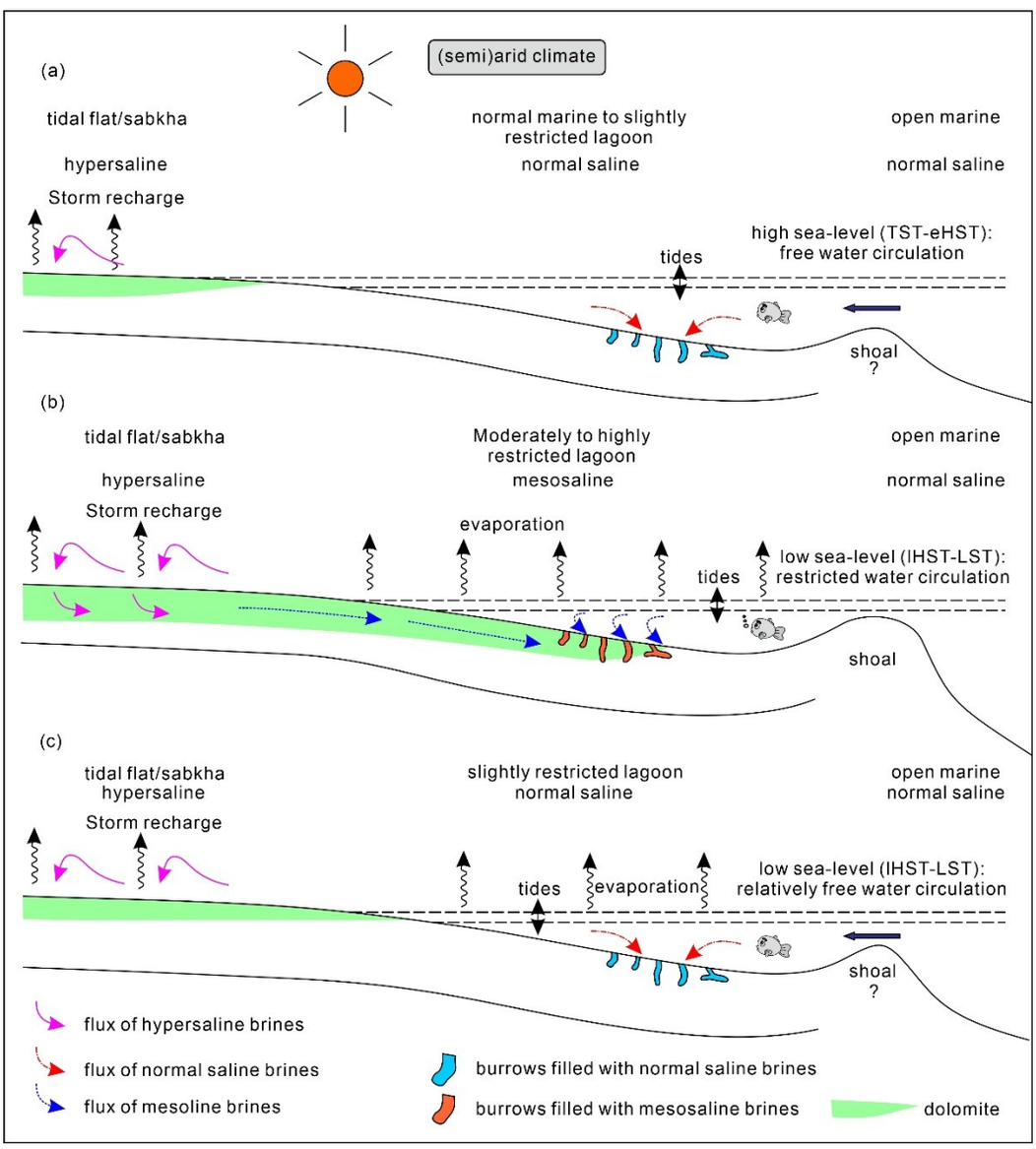

Figure 16. Schematic map explaining the observed dolomitization patterns in the study area. (a) During relatively high sea-level, relatively free water circulation took place between lagoon and the open ocean. Reflux dolomitization may occur in shallow lagoonal settings near the coastal line; lagoon was occupied by seawater with normal salinities and extensive burrows were likely produced by burrowing organisms. (b) During relatively low sea-level, reflux dolomitization may be viable in not completely consolidated lagoonal lime muds. The water circulation between lagoon and the open ocean became limited to a relative extent due to barrier effects of platform rim; highly restricted or semi-restricted lagoon was characterized by mesosaline brines and antecedent burrows were filled with mesosaline brines channeling through networks of burrows. (c) During relatively low sea-level, the water circulation of lagoon to the open ocean still was free due to lack of effective barrier shoal, which resembled the conditions of relatively high sea-level.

over, these burrows maintained a particular geochemical microenvironment, which might occur as a few cm-scale zone extending into sediment substrates (Gingras et al., 2004b). In addition, burrows also could render excellent substrates for bacterial colonization because of localized, concentrated organic material in the form of mucous or faecal material within burrow linings (Gingras et al., 2004b). There were masses of free SO_{2-4} ions present within the oxic to suboxic sub-environments, which probably hamper the precipitation of dolomite (Slaughter and Hill, 1991; Hardie, 1987) and lower the Mg/Ca ratio through binding with Mg^{2+} (Gingras et al., 2004b). It has been suggested that dolomite can be preferentially formed by the microbe mediation (e.g., sulfate reduction bacteria as indicated by the presence of framboidal pyrites; Figure 8h) under reducing conditions (Wright and Wacey, 2005; van Lith et al., 2003; Vasconcelos and McKenzie, 1997; Vasconcelos et al., 1995). Within burrow microenvironments, there was an anoxic zone characterized by abundant CO_2 and NH_3, common products in the geochemical setting (Gingras et al., 2004b). The reaction of ammonia with water ($NH_3 + H_2O \rightarrow NH_4^+ + OH^-$) effectively raises the pH of the interstitial fluids in and around the burrow networks, which, in turn, increase the activities of the bicarbonate ions (HCO_3^-), facilitating the direct dolomite precipitation (Gingras et al., 2004b). Under reducing conditions, the combination of elevating pH and decreasing sulfate ions consumed by sulfate-reducing bacteria (indicated by the presence of framboidal pyrite; Figure 8h) is crucial to the precipitation of dolomite within burrow networks in the submarine and/or shallow burial conditions (Baldermann et al., 2015; Gingras et al., 2004b). Thus, this geochemical microenvironment is a favorable site for the precipitation of dolomite facilitated by microbe mediation (Gingras et al., 2004b; van Lith et al., 2003). In addition, the cation enrichment on burrow linings were mobile and migrated forth and back between anoxic and oxic zones. These locally-concentrated cations in concert with the Mg^{2+} from interstitial waters (aforementioned mesosaline to penesaline brines) channeling primarily through networks of burrows offer a likely local source of Mg^{2+} for dolomitization, also promoting dolomite precipitation (Mirsal and Zankl, 1985). Moreover, dolomite precipitation may extend from the margins of burrows into the surrounding matrix limestones, forming mm-thick dolomitic zones composed of floating dolomite rhomb crystals. It is noted that limestones with dolomitized burrows probably may be subject to massive reflux dolomitization concurrently or later, leading to the complete replacement of limestones by dolomites (Figure 16b).

5.1.2 Origin of burrow-associated calcites

As mentioned above, the formation of burrow-associated carbonates was closely associated with lagoonal environments with variably restricted water exchange with open ocean. In contrast to BADs, the stratigraphic distribution (in the upper part of the Yingshan Formation) of BACs and their close relationship with relatively higher sea-level conditions with rare early-forming dolomites (Figure 6) indicate that the BACs in western Tarim Basin were likely formed in restriction-improved settings that were not favorable for early dolomite development. Additionally, the good correlation between the occurrence of BACs and the transgression of long-term (e.g., second-order) depositional sequences (Figure 6) suggests that the formation of BACs was dictated by long-term sea-level variations on a larger scale. Moreover, the BACs preferentially occur in the lower – middle part of meter-scale cycles, pointing to the close association of BAC development with high-frequency sea-level fluctuations. In contrast to western Tarim Basin, the BACs were not encountered in the covered intervals of drilling wells from the subsurface of northern and central Tarim Basin (Figure 7), also suggesting the development of BACs is also determined jointly by sea-level variations of variable orders and paleo-topography (depositional environments), similar to the BADs (see Section 5.1.1).

The non-luminescence of BACs points to a reducing condition where Fe^{2+} ions were extensively present (Richter et al., 2003; Machel, 1985). The $\delta^{13}C$ values (-1.6‰ and -1.1‰ VPDB) of BACs are in agreement with those of their surrounding limestones (-1.6‰ to -0.9‰ VPDB) and brachiopods (-3.0‰ to 0 VPDB; Shields et al., 2003; Veizer et al., 1999; Qing and Veizer, 1994) precipitated from coeval seawater, indicating their formation in equilibrium with seawater-derived brines. Taking into consideration their slightly higher precipitation temperatures than matrix limestones, the $\delta^{18}O$ values (-8.1‰ and -7.6‰ VPDB) of BACs are comparable to those of (-7.8‰ to -7.0‰ VPDB) of the surrounding limestones, also pointing out their seawater origin.

5.2 Origin of Early-Stage Calcite Cements

The early-stage calcite cements commonly occluded completely or partially the porosity of BADs in the Tarim Basin (Figures 4c and 8e–8h), but predated the emplacement of hydrocarbons that were derived from the Cambrian to Lower Ordovician source rocks (Yang et al., 2011). Under this circumstance, the precipitation of early-stage calcite cements from the pore water after the BAD development could have been ceased due to the hydrocarbon charge (e.g., Guo et al., 2016; Tucker and Wright, 1990) from the underlying source rocks of the Cambrian to Lower Ordovician (Yang et al., 2011). This process may lead to the preservation of residual porosity after the precipitation of early-stage calcite cements. The $\delta^{13}C$ values (-2.0‰ to -0.7‰ VPDB) of early-stage calcite cements are comparable to those of surrounding micritic limestones and brachiopods precipitated in equilibrium with coeval seawater (Figure 10) (Shields et al., 2003; Veizer et al., 1999; Qing and Veizer, 1994), indicating they were formed from seawater-derived fluids. Applying the calcite-water oxygen-isotope fractionation equation of Land (1983), the $\delta^{18}O$ values of parental fluids of early-stage calcite cements vary from +1.5‰ to +5.5‰ VSMOW (Fig-

ure 15) on the basis of their $\delta^{18}O$ values (-9.2‰ to -7.1‰ VPDB) and T_h values (77.7–93.4 ºC). The estimated $\delta^{18}O$ values of fluids from which early-stage calcite cements were precipitated are much higher than those of coeval seawater (-7.4‰ to -4.7‰ VSMOW) and parental fluids (-7.5‰ to +1.8‰ VSMOW) of the BADs in the Tarim Basin (Figure 15), indicating a drastic concentration of ^{18}O in fluids. It has been suggested that the enrichment of ^{18}O in fluids could be caused by evaporation and/or fluid-rock interaction (e.g., Dong et al., 2017; Gregg et al., 2015; Jiang et al., 2013; Machel, 2004; Warren, 2000; Budd, 1997). The petrographic evidence of matrix and burrow-associated dolomites (see Section 4.2), however, has ruled out the possibility of evaporation-induced ^{18}O enrichment. Thus, fluid-rock interaction during progressive burial was likely a viable mechanism accounting for the concentration of ^{18}O in fluids responsible for early-stage calcite cement precipitation.

5.3 Reservoir Implications

In the past, the dolomitization process was considered to improve the porosity and permeability of carbonate reservoirs due to the volume decrease of resultant dolomites relative to their precursor limestones (Weyl, 1960). However, numerous studies have later revealed that the dolomitization process does not necessarily lead to an advance in petrophysical properties (e.g., Machel, 2004; Warren, 2000; Saller and Henderson, 1998; Lucia and Major, 1994). The impact of dolomitization on porosity and permeability of carbonate reservoirs is complicatedly governed by the combination of source and quantity of magnesium ions, hydrological driving mechanism, geochemical properties of dolomitizing fluids, and other factors (Saller and Henderson, 1998; Land, 1985).

Although the BADs have been reported as effective hydrocarbon reservoirs (e.g., Golab et al., 2017; Baniak et al., 2013, 2014; Gingras et al., 2004a), this type of dolomite within the Yingshan Formation shows distinctive petrophysical properties. As mentioned above (see Section 4.2), the BADs in dolomitized intervals in western and central Tarim Basin have better reservoir properties than those hosted in matrix limestones (Figures 4 and 8). In addition, the BADs in the northern part of the basin are also present in micritic limestones but display low reservoir potential (Figures 8c and 8d). The variation in petrophysical properties of the BADs in different parts of the Tarim Basin is most likely ascribed to their different diagenetic histories that they have undergone (Figure 9). Petrographic and geochemical evidence suggest that burrow-associated carbonates were formed in near-surface to shallow burial settings. In western and central Tarim Basin, the overgrowth of BAD crystals was followed by early-stage calcite cement (C2) (Figures 8e, 8f, 8g, 9), which was probably sourced from dissolution and re-precipitation of host limestones during deeper burial. Afterward, the precipitation of early-stage calcite cements was finally ceased due to the emplacement of hydrocarbon from the underlying source rocks of the Cambrian to Lower Ordovician Age (Yang et al., 2011), leading to the retainment of relic intercrystalline porosity (Figures 4c, 8g, 8h). Meanwhile, the dissolution of BADs could have been operative by acidic fluids derived from the maturing process of source rocks as evidenced by corroded edges of dolomite crystals (Figures 8g and 8h). In contrast, the BADs in northern Tarim Basin are mainly characterized by tightly-packed crystals (Figures 8c–8f), which is attributed to the continuous overgrowth of dolomite crystals owing to the absence of hydrocarbon emplacement.

Overall, only could porous BADs serve as potential reservoirs for hydrocarbons. Burrow-related, selective dolomitization, however, developed distinctive textural heterogeneity, which was manifested by chaotically distributed, permeable conduits (burrows) and tortuous flow paths (Baniak et al., 2013; Gingras et al., 2004a). This heterogeneity made reservoir development complicated and formed a dual-porosity and dual-permeability system (Gingras et al., 2004a). In addition, the stratigraphic distributional heterogeneity also makes it difficult to predict the spatial and temporal distribution of the BAD reservoirs. Therefore, although the BADs can act as potential reservoirs for hydrocarbons, the prediction of their distribution still needs further studies.

6 CONCLUSIONS

Based on detailed field and core investigations, petrographic, and isotopic (C-O-Sr) geochemical analyses, and fluid inclusion microthermometry on the burrow-associated carbonates of the Lower–Middle Ordovician Yingshan Formation in the Tarim Basin, main conclusions are drawn as follows.

(1) The development of burrow-associated carbonates was likely controlled by the interaction of sea-level oscillations of variable orders and paleogeography (depositional facies).

(2) The dolomitizing fluids responsible for the precipitation of the BADs in the Tarim Basin are probably characterized by slightly evaporated (i.e., mesosaline to penesaline) seawater, whereas the parental fluids of BACs are likely represented by nearly normal seawater.

(3) In addition to anoxic conditions, the presence of sulfate-reducing bacteria, the occurrence of marine-sourced organic matter, and a sufficient supply of magnesium, other factors (i.e., Mg^{2+} concentration) may also determine the formation of BADs.

(4) The relatively porous BADs develop a dual-porosity and dual-permeability system due to heterogeneity and occur as potential reservoirs for hydrocarbons in the Tarim Basin. Their development was likely ascribed to the emplacement of hydrocarbons from underlying source rocks of the Cambrian to Lower Ordovician.

ACKNOWLEDGMENTS

This study was jointly supported by Guizhou Provincial Science and Technology Projects (No. ZK[2021] ordinary 199), the National Natural Science Foundation of

China (Nos. 42262019, 92062221), and the National Key R&D Program of China (No. 2017YFC0603103). We thank Linlin Cui, Chaofeng Li, and Youlian Li (Institute of Geology and Geophysics, CAS) for their assistance in geochemical analyses. Sincere thanks also go to Dr. Shaofeng Dong, Dr. Yi Ding, and Dr. Donghua You for their assistance in the fieldwork and in the borehole core observation in Northwest Exploration and Production Company, SINOPEC. We would like to express our sincere gratitude to the two anonymous reviewers for their constructive feedback and critical comments, which significantly contributed to improving the earlier version of this manuscript. We also extend our appreciation to the editor for the professional oversight throughout the review process. The final publication is available at Springer via https://doi.org/10.1007/s12583-022-1673-6.

Electronic Supplementary Materials: Supplementary material (Table S1) is available in the online version of this article at https://doi.org/10.1007/s12583-022-1673-6.

Conflict of Interest

The authors declare that they have no conflict of interest.

REFERENCES CITED

Adams, J. E., Rhodes, M. L., 1960. Dolomitization by Seepage Refluxion. *AAPG Bulletin*, 44: 1912–1920. https://doi.org/10.1306/0bda6263-16bd-11d7-8645000102c1865d

Al-Aasm, I. S., Taylor, B. E., South, B., 1990. Stable Isotope Analysis of Multiple Carbonate Samples Using Selective Acid Extraction. *Chemical Geology*: *Isotope Geoscience Section*, 80(2): 119 – 125. https://doi.org/10.1016/0168-9622(90)90020-D

Baker, P. A., Burns, S. J., 1985. Occurrence and Formation of Dolomite in Organic-Rich Continental Margin Sediments. *AAPG Bulletin*, 69: 1917–1930. https://doi.org/10.1306/94885570-1704-11d7-8645000102c1865d

Baldermann, A., Deditius, A. P., Dietzel, M., et al., 2015. The Role of Bacterial Sulfate Reduction during Dolomite Precipitation: Implications from Upper Jurassic Platform Carbonates. *Chemical Geology*, 412: 1–14. https://doi.org/10.1016/j.chemgeo.2015.07.020

Baniak, G. M., Amskold, L., Konhauser, K. O., et al., 2014. Sabkha and Burrow-Mediated Dolomitization in the Mississippian Debolt Formation, Northwestern Alberta, Canada. *Ichnos*, 21(3): 158 – 174. https://doi.org/10.1080/10420940.2014.930036

Baniak, G. M., Gingras, M. K., Pemberton, S. G., 2013. Reservoir Characterization of Burrow-Associated Dolomites in the Upper Devonian Wabamun Group, Pine Creek Gas Field, Central Alberta, Canada. *Marine and Petroleum Geology*, 48: 275–292. https://doi.org/10.1016/j.marpetgeo.2013.08.020

Banner, J. L., 1995. Application of the Trace Element and Isotope Geochemistry of Strontium to Studies of Carbonate Diagenesis. *Sedimentology*, 42(5): 805 – 824. https://doi.org/10.1111/j.1365-3091.1995.tb00410.x

Banner, J. L., Hanson, G. N., 1990. Calculation of Simultaneous Isotopic and Trace Element Variations during Water-Rock Interaction with Applications to Carbonate Diagenesis. *Geochimica et Cosmochimica Acta*, 54(11): 3123–3137. https://doi.org/10.1016/0016-7037(90)90128-8

Bontognali, T. R. R., Vasconcelos, C., Warthmann, R. J., et al., 2010. Dolomite Formation within Microbial Mats in the Coastal Sabkha of Abu Dhabi (United Arab Emirates). *Sedimentology*, 57(3): 824–844. https://doi.org/10.1111/j.1365-3091.2009.01121.x

Bromley, R. G., 1996. Trace Fossils: Biology, Taphonomy and Applications (2nd Edition). Routledge, Chapman & Hall, London

Budd, D. A., 1997. Cenozoic Dolomites of Carbonate Islands: Their Attributes and Origin. *Earth-Science Reviews*, 42(1/2): 1 – 47. https://doi.org/10.1016/S0012-8252(96)00051-7

Burke, W. H., Denison, R. E., Hetherington, E. A., et al., 1982. Variation of Seawater $^{87}Sr/^{86}Sr$ Throughout Phanerozoic Time. *Geology*, 10(10): 516 – 519. https://doi.org/10.1130/0091-7613(1982)10<516:vosstp>2.0.co;2

Chen, D. Z., Qing, H. R., Yang, C., 2004. Multistage Hydrothermal Dolomites in the Middle Devonian (Givetian) Carbonates from the Guilin Area, South China. *Sedimentology*, 51(5): 1029–1051. https://doi.org/10.1111/j.1365-3091.2004.00659.x

Chow, N., Longstaffe, F. J., 1995. Dolomites of the Middle Devonian Elm Point Formation, Southern Manitoba: Intrinsic Controls on Early Dolomitization. *Bulletin of Canadian Petroleum Geology*, 43: 214–225. https://doi.org/10.35767/gscpgbull.43.2.214

Coplen, T. B., Kendall, C., Hopple, J., 1983. Comparison of Stable Isotope Reference Samples. *Nature*, 302: 236–238. https://doi.org/10.1038/302236a0

Corlett, H. J., Jones, B., 2012. Petrographic and Geochemical Contrasts between Calcite- and Dolomite-Filled Burrows in the Middle Devonian Lonely Bay Formation, Northwest Territories, Canada: Implications for Dolomite Formation in Paleozoic Burrows. *Journal of Sedimentary Research*, 82(9): 648 – 663. https://doi.org/10.2110/jsr.2012.57

Davies, G. R., Smith, L. B., Jr., 2006. Structurally Controlled Hydrothermal Dolomite Reservoir Facies: An Overview. *AAPG Bulletin*, 90(11): 1641–1690. https://doi.org/10.1306/05220605164

Dickson, J. A. D., 1966. Carbonate Identification and Genesis as Revealed by Staining. *SEPM Journal of Sedimentary Research*, 36: 491 – 505. https://doi.org/10.1306/74d714f6-2b21-11d7-8648000102c1865d

Ding, Y., Chen, D. Z., Zhou, X. Q., et al., 2020. Paired $\delta^{13}C_{carb}$-$\delta^{13}C_{org}$ Evolution of the Dengying Formation from Northeastern Guizhou and Implications for Stratigraphic Correlation and the Late Ediacaran Carbon Cycle. *Journal of Earth Science*, 31(2): 342–353. https://doi.org/10.1007/s12583-018-0886-1

Dong, S. F., Chen, D. Z., Qing, H. R., et al., 2013. Hydrothermal Alteration of Dolostones in the Lower Ordovician, Tarim Basin, NW China: Multiple Constraints from Petrology, Isotope Geochemistry and Fluid Inclusion Microthermometry. *Marine and Petroleum Geology*, 46: 270–286. https://doi.org/10.1016/j.marpetgeo.2013.06.013

Dong, S. F., Chen, D. Z., Zhou, X. Q., et al., 2017. Tectonically Driven Dolomitization of Cambrian to Lower Ordovician Carbonates of the Quruqtagh Area, North-Eastern Flank of Tarim Basin, North-West China. *Sedimentology*, 64(4): 1079 – 1106. https://doi.org/10.1111/sed.12341

Donovan, S. K., 1994. The Palaeobiology of Trace Fossils. Johns Hopkins University Press, Baltimore

Ekdale, A. A., Muller, L. N., Novak, M. T., 1984. Quantitative Ichnology of Modern Pelagic Deposits in the Abyssal Atlantic. *Palaeogeography*, *Palaeoclimatology*, *Palaeoecology*, 45(2): 189–223. https://doi.org/10.1016/0031-0182(84)90040-3

Fabricius, I. L., Borre, M. K., 2007. Stylolites, Porosity, Depositional Texture, and Silicates in Chalk Facies Sediments. Ontong Java Plateau-Gorm and Tyra Fields, North Sea. *Sedimentology*, 54 (1): 183–205. https://doi.org/10.1111/j.1365-3091.2006.00828.x

Fang, D. J. , Shen, Z. Y., 2001. Panerozoic Apparent Polarander Paths of Tarim and Plate Motion. *Journal of Zhejiang University*: *Science Edition*, 28(1): 100–106 (in Chinese with English Abstract)

Feng, Z. Z., Bao, Z. D., Wu, M. B., et al., 2007. Lithofacies Palaeogeography of the Ordovician in Tarim Area. *Journal of Palaeogeography*, 9(5): 447–460 (in Chinese with English Abstract)

Flügel, E., 2004. Microfacies of Carbonate Rocks: Analysis, Interpretation and Application. Springer Berlin Heidelberg, Berlin, Heidelberg. 984. https://doi.org/10.1007/978-3-642-03796-2

Folk, R. L., Land, L. S., 1975. Mg/Ca Ratio and Salinity: Two Controls over Crystallization of Dolomite. *AAPG Bulletin*, 59: 60–68. https://doi.org/10.1306/83d91c0e-16c7-11d7-8645000102c1865d

Fu, Q. L., Qing, H. R., Bergman, K. M., 2006. Dolomitization of the Middle Devonian Winnipegosis Carbonates in South-Central Saskatchewan, Canada. *Sedimentology*, 53(4): 825–848. https://doi.org/10.1111/j.1365-3091.2006.00794.x

Gao, D., Lin, C. S., Huang, L. L., et al., 2021. Depositional Facies and Diagenesis of the Lianglitage Formation in Northwestern Tazhong Uplift, Tarim Basin, China: Implications for the Genesis of Ultra-Deep Limestone Reservoir. *Arabian Journal of Geosciences*, 14(9): 750. https://doi.org/10.1007/s12517-021-07080-9

Gao, Z. Q., Fan, T. L., Jiao, Z. F., et al., 2006. The Structural Types and Depositional Characteristics of Carbonate Platform in the Cambrian – Ordovician of Tarim Basin. *Acta Sedimentologica Sinica*, 24(1): 19–27 (in Chinese with English Abstract)

Gingras, M. K., Mendoza, C. A., Pemberton, S. G., 2004a. Fossilized Worm Burrows Influence the Resource Quality of Porous Media. *AAPG Bulletin*, 88(7): 875–883. https://doi.org/10.1306/01260403065

Gingras, M. K., Pemberton, S. G., Muelenbachs, K., et al., 2004b. Conceptual Models for Burrow-Related, Selective Dolomitization with Textural and Isotopic Evidence from the Tyndall Stone, Canada. *Geobiology*, 2(1): 21–30. https://doi.org/10.1111/j.1472-4677.2004.00022.x

Golab, J. A., Smith, J. J., Clark, A. K., et al., 2017. Bioturbation-Influenced Fluid Pathways within a Carbonate Platform System: The Lower Cretaceous (Aptian – Albian) Glen Rose Limestone. *Palaeogeography*, *Palaeoclimatology*, *Palaeoecology*, 465: 138–155. https://doi.org/10.1016/j.palaeo.2016.10.025

Goldstein, R. H., 2001. Fluid Inclusions in Sedimentary and Diagenetic Systems. *Lithos*, 55(1/2/3/4): 159 – 193. https://doi.org/10.1016/S0024-4937(00)00044-X

Gregg, J. M., Bish, D. L., Kaczmarek, S. E., et al., 2015. Mineralogy, Nucleation and Growth of Dolomite in the Laboratory and Sedimentary Environment: A Review. *Sedimentology*, 62(6): 1749–1769. https://doi.org/10.1111/sed.12202

Gregg, J. M., Shelton, K. L., 1990. Dolomitization and Dolomite Neomorphism in the Back Reef Facies of the Bonneterre and Davis Formations (Cambrian), Southeastern Missouri. *SEPM Journal of Sedimentary Research*, 60: 549–562. https://doi.org/10.1306/212f91e2-2b24-11d7-8648000102c1865d

Gregg, J. M., Sibley, D. F., 1984. Epigenetic Dolomitization and the Origin of Xenotopic Dolomite Texture. *SEPM Journal of Sedimentary Research*, 54: 908 – 931. https://doi.org/10.1306/212f8535-2b24-11d7-8648000102c1865d

Gu, J., Chou, J., Yan, H., et al. 1994. Sedimentary Facies and Petroleum Accumulations: Petroleum Exploration in the Tarim Basin. Petroleum Industry Press, Beijing (in Chinese)

Guo, C., Chen, D. Z., Dong, S. F., et al., 2017. Early Dolomitisation of the Lower–Middle Ordovician Cyclic Carbonates in Northern Tarim Basin, NW China. *Science China Earth Sciences*, 60(7): 1283–1298. https://doi.org/10.1007/s11430-017-9056-1

Guo, C., Chen, D. Z., Qing, H. R., et al., 2016. Multiple Dolomitization and Later Hydrothermal Alteration on the Upper Cambrian–Lower Ordovician Carbonates in the Northern Tarim Basin, China. *Marine and Petroleum Geology*, 72: 295 – 316. https://doi.org/10.1016/j.marpetgeo.2016.01.023

Guo, C., Chen, D. Z., Qing, H. R., et al., 2020. Early Dolomitization and Recrystallization of the Lower-Middle Ordovician Carbonates in Western Tarim Basin (NW China). *Marine and Petroleum Geology*, 111: 332–349. https://doi.org/10.1016/j.marpetgeo.2019.08.017

Guo, C., Chen, D. Z., Song, Y. F., et al., 2018a. Depositional Environments and Cyclicity of the Early Ordovician Carbonate Ramp in the Western Tarim Basin (NW China). *Journal of Asian Earth Sciences*, 158: 29–48. https://doi.org/10.1016/j.jseaes.2018.02.006

Guo, C., Chen, D. Z., Zhou, X. Q., et al., 2018b. Depositional Facies and Cyclic Patterns in a Subtidal-Dominated Ramp during the Early – Middle Ordovician in the Western Tarim Basin (NW China). *Facies*, 64(3): 16. https://doi.org/10.1007/s10347-018-0529-0

Guo, F., Lai, S. H., Guo, L., 2010. Ordovician Sequence Stratigraphy and Sedimentology in the Dabantage Area, Tarim Basin. *Journal of Stratigraphy*, 34(2): 135 – 144. https://doi.org/10.19839/j.cnki.dcxzz.2010.02.003 (in Chinese with English Abstract)

Haley, B. A., Klinkhammer, G. P., McManus, J., 2004. Rare Earth Elements in Pore Waters of Marine Sediments. *Geochimica et Cosmochimica Acta*, 68(6): 1265–1279. https://doi.org/10.1016/j.gca.2003.09.012

Hardie, L. A., 1987. Dolomitization: A Critical View of Some Current Views. *Journal of Sedimentary Research*, 57(1): 166–183. https://doi.org/10.1306/212f8ad5-2b24-11d7-8648000102c1865d

He, Y., Li, W. Q., Liu, H. C., et al., 2025. Petrogenesis of the Dengying Formation Dolomite in Northeast Sichuan Basin, SW China: Constraints from Carbon-Oxygen Isotopic and Trace Elemental Data. *Journal of Earth Science*, 36(1): 75–88. https://doi.org/10.1007/s12583-022-1732-z

He, Z., Mao, H., Zhou, X., et al., 2000. Complex Petroleum System and Muticycle Basin in Tarim. *Oil & Gas Geology*, 21: 207–213 (in Chinese with English Abstract)

Horbury, A. D., Qing, H. R., 2004. 'Pseudobreccias' Revealed as Calcrete Mottling and Bioturbation in the Late Dinantian of the

Southern Lake District, UK. *Sedimentology*, 51(1): 19–38. https://doi.org/10.1046/j.1365-3091.2003.00607.x

Hu, M. Y., Hu, Z. G., Li, S. T., et al., 2011. Geochemical Characteristics and Genetic Mechanism of the Ordovician Dolostone in the Tazhong Area, Tarim Basin. *Acta Geologica Sinica*, 85(12): 2060–2069 (in Chinese with English Abstract)

Hu, M. Y., Ngia, N. R., Gao, D., 2019. Dolomitization and Hydrotectonic Model of Burial Dolomitization of the Furongian-Lower Ordovician Carbonates in the Tazhong Uplift, Central Tarim Basin, NW China: Implications from Petrography and Geochemistry. *Marine and Petroleum Geology*, 106: 88 – 115. https://doi.org/10.1016/j.marpetgeo.2019.04.018

Jia, C. Z., Wei, G. Q., 2002. Structural Characteristics and Hydrocarbon of Tarim Basin. *Chinese Science Bulletin*, 47(S1): 1–8 (in Chinese)

Jia, L. Q., Cai, C. F., Jiang, L., et al., 2016. Petrological and Geochemical Constraints on Diagenesis and Deep Burial Dissolution of the Ordovician Carbonate Reservoirs in the Tazhong Area, Tarim Basin, NW China. *Marine and Petroleum Geology*, 78: 271–290. https://doi.org/10.1016/j.marpetgeo.2016.09.031

Jiang, L., Cai, C. F., Worden, R. H., et al., 2013. Reflux Dolomitization of the Upper Permian Changxing Formation and the Lower Triassic Feixianguan Formation, NE Sichuan Basin, China. *Geofluids*, 13(2): 232–245. https://doi.org/10.1111/gfl.12034

Jiang, L., Cai, C. F., Worden, R. H., et al., 2016. Multiphase Dolomitization of Deeply Buried Cambrian Petroleum Reservoirs, Tarim Basin, North-West China. *Sedimentology*, 63 (7): 2130–2157. https://doi.org/10.1111/sed.12300

Jin, Z. J., Zhu, D. Y., Hu, W. X., et al., 2006. Geological and Geochemical Signatures of Hydrothermal Activity and Their Influence on Carbonate Reservoir Beds in the Tarim Basin. *Acta Geologica Sinica*, 80(2): 245–253, 314 (in Chinese with English Abstract).

Jones, G. D., Whitaker, F., Smart, P., et al., 2000. Numerical Modelling of Geothermal and Reflux Circulation in Enewetak Atoll: Implications for Dolomitization. *Journal of Geochemical Exploration*, 69: 71 – 75. https://doi.org/10.1016/S0375-6742(00)00010-8

Kaufman, J., 1994. Numerical Models of Fluid Flow in Carbonate Platforms: Implications for Dolomitization. *SEPM Journal of Sedimentary Research*, 64: 128 – 139. https://doi.org/10.1306/d4267d2f-2b26-11d7-8648000102c1865d

Kerans, C., 1988. Karst-Controlled Reservoir Heterogeneity in Ellenburger Group Carbonates of West Texas. *AAPG Bulletin*, 72: 1160–1183. https://doi.org/10.1306/703c996f-1707-11d7-8645000102c1865d

Kohout, F. A., Henry, H. R., Banks, J. E., 1977. Hydrogeology Related to Geothermal Conditions of the Floridan Plateau, In: Smith, K. L., Griffin, G. M., eds., The Geothermal Nature of the Floridan Plateau. Florida Department of Natural Resources Bureau: Geological Special Publication, 21: 1–34

Kupecz, J. A., Land, L. S., 1991. Late-Stage Dolomitization of the Lower Ordovician Ellenburger Group, West Texas. *SEPM Journal of Sedimentary Research*, 61: 551 – 574. https://doi.org/10.1306/d426775d-2b26-11d7-8648000102c1865d

Lan, X. D., Liu, H., Lü, X. X., et al., 2018. Dolomites of the Yingshan Formation in the Tazhong Low Rise, Tarim Basin: Dolomitisation and Reformation Model. *Geosciences Journal*, 22(1): 47 – 64. https://doi.org/10.1007/s12303-017-0027-3

Land, L. S., 1980. The Isotopic and Trace Element Geochemistry of Dolomite: The State of the Art. In: Zenger, D. H., Dunham, J. B., Ethington, R. L. eds., Concepts and Models of Dolomitization. *SEPM Special Publication*, 28: 87–110

Land, L. S., 1983. The Application of Stable Isotopes to Studies of the Origin of Dolomite and to Problems of Diagenesis of Clastic Sediments. In: Arthur, M. A., Anderson, T. F., Kaplan, I. R., et al., eds., Stable Isotopes in the Sedimentary Geology. SEPM Short Course Notes, 10: 4.1–4.22

Land, L. S., 1985. The Origin of Massive Dolomite. *Journal of Geological Education*, 33(2): 112 – 125. https://doi.org/10.5408/0022-1368-33.2.112

Li, H. L., Qiu, N. S., Jin, Z. J., et al., 2005. Geothermal History of Tarim Basin. *Oil & Gas Geology*, 26(5): 613 – 617 (in Chinese with English Abstract)

Li, K., Cai, C., He, H., et al., 2011. Origin of Palaeo-Waters in the Ordovician Carbonates in Tahe Oilfield, Tarim Basin: Constraints from Fluid Inclusions and Sr, C and O Isotopes. *Geofluids*, 11 (1): 71–86. https://doi.org/10.1111/j.1468-8123.2010.00312.x

Li, Y., Li, Q., Zhang, H., et al., 1995. Palaeomagnetic Study of Tarim and Its Adjacent Area as Well as the Formation and Evolution of Tarim Basin. *Xijiang Geology*, 13(4): 293 – 376 (in Chinese with English Abstract)

Lin, C. S., Yang, H. J., Cai, Z. Z., et al., 2013. Evolution of Depositional Architecture of the Ordovician Carbonate Platform in the Tarim Basin and Its Response to Basin Processes. *Acta Sedimentologica Sinica*, 31(5): 907–919. https://doi.org/10.14027/j.cnki.cjxb.2013.05.017 (in Chinese with English Abstract)

Lucia, F. J., Major, R., 1994. Porosity Evolution through Hypersaline Reflux Dolomitization. In: Purser, B. H., Tucker, M. E., Zenger, D. H., eds., Dolomites: A Volume in Honor of Dolomieu. The International Association of Sedimentologists: Special Publication, 21: 325–341

Machel, H. G., 1985. Cathodoluminescence in Calcite and Dolomite and Its Chemical Interpretation. *Geoscience Canada*, 12: 139 – 147. https://journals.lib.unb.ca/index.php/GC/article/view/3427

Machel, H. G., 1997. Recrystallization Versus Neomorphism, and the Concept of ‘Significant Recrystallization’ in Dolomite Research. *Sedimentary Geology*, 113(3/4): 161–168. https://doi.org/10.1016/S0037-0738(97)00078-X

Machel, H. G., 2004. Concepts and Models of Dolomitization: A Critical Reappraisal. In: Braithwaite, C. J. R., Rizzi, G., Darke, G., eds., The Geometry and Petrogenesis of Dolomite Hydrocarbon Reservoirs. *Geological Society*, *London*, *Special Publications*, 235(1): 7–63. https://doi.org/10.1144/gsl.sp.2004.235.01.02

Malone, M. J., Baker, P. A., Burns, S. J., 1996. Hydrothermal Dolomitization and Recrystallization of Dolomite Breccias from the Miocene Monterey Formation, Tepusquet Area, California. *SEPM Journal of Sedimentary Research*, 66: 976 – 990. https://doi.org/10.1306/d426845a-2b26-11d7-8648000102c1865d

Mattes, B. W., Mountjoy, E. W., 1980. Burial Dolomitization of the Upper Devonian Miette Buildup, Jasper National Park, Alberta. In: Zenger, D. H., Dunham, J. B., Ethington, R. L., eds.,

Concepts and Models of Dolomitization. SEPM Special Publication, 28: 259–297. https://doi.org/10.2110/pec.80.28.0259

Mazzullo, S. J., 2000. Organogenic Dolomitization in Peritidal to Deep-Sea Sediments: PERSPECTIVES. *SEPM Journal of Sedimentary Research*, 70: 10–23. https://doi.org/10.1306/d4268b71-2b26-11d7-8648000102c1865d

McCrea, J. M., 1950. On the Isotopic Chemistry of Carbonates and a Paleotemperature Scale. *The Journal of Chemical Physics*, 18 (6): 849–857. https://doi.org/10.1063/1.1747785

Meister, P., McKenzie, J. A., Vasconcelos, C., et al., 2007. Dolomite Formation in the Dynamic Deep Biosphere: Results from the Peru Margin. *Sedimentology*, 54(5): 1007–1032. https://doi.org/10.1111/j.1365-3091.2007.00870.x

Mirsal, I. A., Zankl, H., 1985. Some Phenomenological Aspects of Carbonate Geochemistry. The Control Effect of Transition Metals. *Geologische Rundschau*, 74: 367–377. https://doi.org/10.1007/bf01824903

Montañez, I. P., Read, J. F., 1992. Fluid-Rock Interaction History during Stabilization of Early Dolomites, Upper Knox Group (Lower Ordovician), U.S. Appalachians. *SEPM Journal of Sedimentary Research*, 62: 753–778. https://doi.org/10.1306/d42679d3-2b26-11d7-8648000102c1865d

Morrow, D. W., 1982. Diagenesis 2. Dolomite-Part 2: Dolomitization Models and Ancient Dolostones. *Geoscience Canada*, 9: 95–107. https://id.erudit.org/iderudit/geocan9_2art01

Mountjoy, E. W., Green, D., Machel, H. G., et al., 1999. Devonian Matrix Dolomites and Deep Burial Carbonate Cements: A Comparison between the Rimbey-Meadowbrook Reef Trend and the Deep Basin of West-Central Alberta. *Bulletin of Canadian Petroleum Geology*, 47(4): 487–509

Mountjoy, E. W., Halim-Dihardja, M. K., 1991. Multiple Phase Fracture and Fault-Controlled Burial Dolomitization, Upper Devonian Wabamun Group, Alberta. *SEPM Journal of Sedimentary Research*, 61: 590–612. https://doi.org/10.1306/d426776c-2b26-11d7-8648000102c1865d

Purser, B. H., Tucker, M. E., Zenger, D. H., 1994. Problems, Progress and Future Research Concerning Dolomites and Dolomitization, In: Purser, B. H., Tucker, M. E., Zenger, D. H, eds., Dolomites. The International Association of Sedimentologists: Special Publication, 21: 3–20

Qiao, Z. F., Shen, A. J., Zheng, J. F., et al., 2012. Classification and Origin of the Lower Ordovician Dolostone in Tarim Basin. *Journal of Palaeogeography* (*Chinese Edition*), 14(1): 21–32 (in Chinese with English Abstract)

Qing, H. R., Bosence, D. W. J., Rose, E. P. F., 2001. Dolomitization by Penesaline Sea Water in Early Jurassic Peritidal Platform Carbonates, Gibraltar, Western Mediterranean. *Sedimentology*, 48(1): 153–163. https://doi.org/10.1046/j.1365-3091.2001.00361.x

Qing, H. R., Veizer, J., 1994. Oxygen and Carbon Isotopic Composition of Ordovician Brachiopods: Implications for Coeval Seawater. *Geochimica et Cosmochimica Acta*, 58(20): 4429–4442. https://doi.org/10.1016/0016-7037(94)90345-X

Qiu, N. S., Chang, J., Zuo, Y. H., et al., 2012. Thermal Evolution and Maturation of Lower Paleozoic Source Rocks in the Tarim Basin, Northwest China. *AAPG Bulletin*, 96(5): 789–821. https://doi.org/10.1306/09071111029

Rameil, N., 2008. Early Diagenetic Dolomitization and Dedolomitization of Late Jurassic and Earliest Cretaceous Platform Carbonates: A Case Study from the Jura Mountains (NW Switzerland, E France). *Sedimentary Geology*, 212(1/2/3/4): 70–85. https://doi.org/10.1016/j.sedgeo.2008.10.004

Ren, P., Lin, C., Han, J., et al., 2015. Microfacies Characteristics and Depositional Evolution of the Lower Ordovician Yingshan Formation in North Slope of Tazhong Area, Tarim Basin. *Natural Gas Geoscience*, 26: 241–251 (in Chinese with English Abstract)

Richter, D. K., Götte, T. H., Götze, J., et al., 2003. Progress in Application of Cathodoluminescence (CL) in Sedimentary Petrology. *Mineralogy and Petrology*, 79(3): 127–166. https://doi.org/10.1007/s00710-003-0237-4

Rosenbaum, J., Sheppard, S. M. F., 1986. An Isotopic Study of Siderites, Dolomites and Ankerites at High Temperatures. *Geochimica et Cosmochimica Acta*, 50(6): 1147–1150. https://doi.org/10.1016/0016-7037(86)90396-0

Saller, A. H., Henderson, N., 1998. Distribution of Porosity and Permeability in Platform Dolomites: Insight from the Permian of West Texas. *AAPG Bulletin*, 82: 1528–1550. https://doi.org/10.1306/1d9bcb01-172d-11d7-8645000102c1865d

Schulz, H. D., Zabel, M., 2006. Marine Geochemistry. Springer-Verlag, New York. https://doi.org/10.1007/3-540-32144-6

Scotese, C. R., McKerrow, W. S., 1990. Revised World Maps and Introduction. *Geological Society*, *London*, *Memoirs*, 12(1): 1–21. https://doi.org/10.1144/gsl.mem.1990.012.01.01

Shao, L., He, H., Peng, S., et al., 2002. Types and Origin of Dolostones of the Cambrian and Ordovician of Bachu Uplift Area in Tarim Basin. *Journal of Palaeogeography*, 4(2): 19–30 (in Chinese with English Abstract)

Shields, G. A., Carden, G. A. F., Veizer, J., et al., 2003. Sr, C, and O Isotope Geochemistry of Ordovician Brachiopods: A Major Isotopic Event around the Middle–Late Ordovician Transition. *Geochimica et Cosmochimica Acta*, 67(11): 2005–2025. https://doi.org/10.1016/S0016-7037(02)01116-X

Sibley, D. F., Gregg, J. M., 1987. Classification of Dolomite Rock Textures. *SEPM Journal of Sedimentary Research*, 57: 967–975. https://doi.org/10.1306/212f8cba-2b24-11d7-8648000102c1865d

Slaughter, M., Hill, R. J., 1991. The Influence of Organic Matter in Organogenic Dolomitization. *Journal of Sedimentary Research*, 61(2): 296–303. https://doi.org/10.1306/d42676f9-2b26-11d7-8648000102c1865d

Sun, S. Q., 1994. A Reappraisal of Dolomite Abundance and Occurrence in the Phanerozoic: PERSPECTIVE. *Journal of Sedimentary Research*, 64A: 396–404. https://doi.org/10.1306/d4267db1-2b26-11d7-8648000102c1865d

Swart, P. K., Burns, S. J., Leder, J. J., 1991. Fractionation of the Stable Isotopes of Oxygen and Carbon in Carbon Dioxide during the Reaction of Calcite with Phosphoric Acid as a Function of Temperature and Technique. *Chemical Geology*: *Isotope Geoscience Section*, 86(2): 89–96. https://doi.org/10.1016/0168-9622(91)90055-2

Tang, L., 1997. Major Evolution Stages of Tarim Basin in Phanerozoic Time. *Earth Science Frontiers*, 4: 318–324 (in Chinese with English Abstract)

Török, A., 2000. Formation of Dolomite Mottling in Middle Triassic Ramp Carbonates (Southern Hungary). *Sedimentary Geology*, 131(3/4): 131–145. https://doi.org/10.1016/S0037-0738(99)

00137-2

Tucker, M. E., Wright, V. P., 1990. Carbonate Sedimentology. Blackwell Scientific Publication, Oxford. 482

van Lith, Y., Warthmann, R., Vasconcelos, C., et al., 2003. Sulphate-Reducing Bacteria Induce Low-Temperature Ca-Dolomite and High Mg-Calcite Formation. *Geobiology*, 1(1): 71–79. https://doi.org/10.1046/j.1472-4669.2003.00003.x

Vasconcelos, C., McKenzie, J. A., 1997. Microbial Mediation of Modern Dolomite Precipitation and Diagenesis under Anoxic Conditions (Lagoa Vermelha, Rio de Janeiro, Brazil). *SEPM Journal of Sedimentary Research*, 67: 378–390. https://doi.org/10.1306/d4268577-2b26-11d7-8648000102c1865d

Vasconcelos, C., McKenzie, J. A., Bernasconi, S., et al., 1995. Microbial Mediation as a Possible Mechanism for Natural Dolomite Formation at Low Temperatures. *Nature*, 377: 220–222. https://doi.org/10.1038/377220a0

Vasconcelos, C., McKenzie, J. A., Warthmann, R., et al., 2005. Calibration of the $\delta^{18}O$ Paleothermometer for Dolomite Precipitated in Microbial Cultures and Natural Environments. *Geology*, 33(4): 317–320. https://doi.org/10.1130/g20992.1

Veizer, J., Ala, D., Azmy, K., et al., 1999. $^{87}Sr/^{86}Sr$, $\delta^{13}C$ and $\delta^{18}O$ Evolution of Phanerozoic Seawater. *Chemical Geology*, 161(1/2/3): 59–88. https://doi.org/10.1016/S0009-2541(99)00081-9

Vinci, F., Iannace, A., Parente, M., et al., 2017. Early Dolomitization in the Lower Cretaceous Shallow-Water Carbonates of Southern Apennines (Italy): Clues about Palaeoclimatic Fluctuations in Western Tethys. *Sedimentary Geology*, 362: 17–36. https://doi.org/10.1016/j.sedgeo.2017.10.007

Wang, Z. H., Qi, Y. P., Bergström, S. M., 2007. Ordovician Conodonts of the Tarim Region, Xinjiang, China: Occurrence and Use as Paleoenvironment Indicators. *Journal of Asian Earth Sciences*, 29(5/6): 832–843. https://doi.org/10.1016/j.jseaes.2006.05.007

Warren, J., 2000. Dolomite: Occurrence, Evolution and Economically Important Associations. *Earth-Science Reviews*, 52(1/2/3): 1–81. https://doi.org/10.1016/S0012-8252(00)00022-2

Weyl, P. K., 1960. Porosity through Dolomitization: Conservation-of-Mass Requirements. *SEPM Journal of Sedimentary Research*, 30: 85–90. https://doi.org/10.1306/74d709cf-2b21-11d7-8648000102c1865d

Wright, D. T., Wacey, D., 2005. Precipitation of Dolomite Using Sulphate-Reducing Bacteria from the Coorong Region, South Australia: Significance and Implications. *Sedimentology*, 52(5): 987–1008. https://doi.org/10.1111/j.1365-3091.2005.00732.x

Yan, W., Wang, X., Wang, Z., et al., 2010. New Evidence on the Sedimentary Framework of the Early Ordovician in Central Tarim and Adjacent Area. *Acta Sedimentologica Sinica*, 28: 1090–1097 (in Chinese with English abstract).

Yang, H. J., Zhu, G. Y., Han, J. F., et al., 2011. Conditions and Mechanism of Hydrocarbon Accumulation in Large Reef-Bank Karst Oil/Gas Fields of Tazhong Area, Tarim Basin. *Acta Petrologica Sinica*, 27: 1865–1885 (in Chinese with English Abstract)

Ye, D., 1994. Deep Dissolution of Cambrian–Ordovician Carbonates in the Northern Tarim Basin. *Acta Sedimentologica Sinica*, 12: 66–71 (in Chinese with English Abstract)

Zenger, D. H., Dunham, J. D., Ethington, R. L., 1980. Concepts and Models of Dolomitization. SEPM Special Publication. 320

Zhang, W., Guan, P., Jian, X., et al., 2014. *In situ* Geochemistry of Lower Paleozoic Dolomites in the Northwestern Tarim Basin: Implications for the Nature, Origin, and Evolution of Diagenetic Fluids. *Geochemistry*, *Geophysics*, *Geosystems*, 15(7): 2744–2764. https://doi.org/10.1002/2013GC005194

Zhang, Y. D., Munnecke, A., 2016. Ordovician Stable Carbon Isotope Stratigraphy in the Tarim Basin, NW China. *Palaeogeography*, *Palaeoclimatology*, *Palaeoecology*, 458: 154–175. https://doi.org/10.1016/j.palaeo.2015.09.001

Zhang, Y. Y., Li, Y., Wang, G., et al., 2017. Windward and Leeward Margins of an Upper Ordovician Carbonate Platform in the Central Tarim Uplift, Xinjiang, Northwestern China. *Palaeogeography*, *Palaeoclimatology*, *Palaeoecology*, 474: 79–88. https://doi.org/10.1016/j.palaeo.2016.12.040

Zhao, Z. J., Zhao, Z., Huang, Z., 2006. Ordovician Conodont Zones and Sedimentary Sequences of the Tarim Basin, Xinjiang, NW China. *Journal of Stratigraphy*, 30: 193–203 (in Chinese with English Abstract)

Zheng, J., Shen, A., Qiao, Z., et al., 2014. Characteristics and Pore Genesis of Dolomite in the Penglaiba Formation in Keping-Bachu Outcrop Area. *Acta Petrolei Sinica*, 35(4): 664–672 (in Chinese with English Abstract)

Zhu, D. Y., Meng, Q. Q., Jin, Z. J., et al., 2015. Formation Mechanism of Deep Cambrian Dolomite Reservoirs in the Tarim Basin, Northwestern China. *Marine and Petroleum Geology*, 59: 232–244. https://doi.org/10.1016/j.marpetgeo.2014.08.022

Zhu, D., Jin, Z., Hu, W., 2010. Hydrothermal Recrystallization of the Lower Ordovician Dolomite and Its Significance to Reservoir in Northern Tarim Basin. *Science China*: *Earth Sciences*, 40: 156–170. https://doi.org/10.1007/s11430-010-0028-9 (in Chinese)